*Acta Oceanol. Sin.*, 2024, Vol. 43, No. 1, P. 80–98
https://doi.org/10.1007/s13131-023-2186-6
http://www.aosocean.com
E-mail: ocean2@hyxb.org.cn

# Simulated Indonesian Throughflow in Makassar Strait across the SODA3 products

Tengfei Xu[1, 2], Zexun Wei[1, 2*], Haifeng Zhao[1], Sheng Guan[1, 2], Shujiang Li[1, 2], Guanlin Wang[1, 2], Fei Teng[1, 2], Yongchui Zhang[3], Jing Wang[4]

[1] First Institute of Oceanography/Key Laboratory of Marine Science and Numerical Modeling, Ministry of Natural Resources, Qingdao 266061, China

[2] Laboratory for Regional Oceanography and Numerical Modeling, Qingdao Marine Science and Technology Center, Qingdao 266237, China

[3] College of Meteorology and Oceanography, National University of Defense Technology, Changsha 410073, China

[4] CAS Key Laboratory of Ocean Circulation and Waves, Center for Ocean Mega-Science, Institute of Oceanology, Chinese Academy of Science, Qingdao 266071, China

Received 23 December 2022; accepted 15 March 2023



**Abstract**

The Indonesian Throughflow (ITF), which connects the tropical Pacific and Indian oceans, plays important roles in the inter-ocean water exchange and regional or even global climate variability. The Makassar Strait is the main inflow passage of the ITF, carrying about 77% of the total ITF volume transport. In this study, we analyze the simulated ITF in the Makassar Strait in the Simple Ocean Data Assimilation version 3 (SODA3) datasets. A total of nine ensemble members of the SODA3 datasets, of which are driven by different surface forcings and bulk formulas, and with or without data assimilation, are used in this study. The annual mean water transports (i.e., volume, heat and freshwater) are related to the combination of surface forcing and bulk formula, as well as whether data assimilation is employed. The phases of the seasonal and interannual variability in water transports cross the Makassar Strait, are basically consistent with each other among the SODA3 ensemble members. The interannual variability in Makassar Strait volume and heat transports are significantly correlated with El Niño-Southern Oscillation (ENSO) at time lags of –6 to 7 months. There is no statistically significant correlation between the freshwater transport and the ENSO. The Makassar Strait water transports are not significantly correlated with the Indian Ocean Dipole (IOD), which may attribute to model deficiency in simulating the propagation of semi-annual Kelvin waves from the Indian Ocean to the Makassar Strait.

**Key words:** Indonesian Throughflow, Simple Ocean Data Assimilation (SODA), El Niño-Southern Oscillation (ENSO), Indian Ocean Dipole (IOD), data assimilation

**Citation:** Xu Tengfei, Wei Zexun, Zhao Haifeng, Guan Sheng, Li Shujiang, Wang Guanlin, Teng Fei, Zhang Yongchui, Wang Jing. 2024. Simulated Indonesian Throughflow in Makassar Strait across the SODA3 products. Acta Oceanologica Sinica, 43(1): 80–98, doi: 10.1007/s13131-023-2186-6

## 1 Introduction

The transport of warm water from the western tropical Pacific to the Indian Ocean, known as the Indonesian Throughflow (ITF), provides the only inter-ocean channel for water mass and heat flux transport at low latitudes, making the so called "great ocean conveyor belt" closed (Broecker, 1991; Gordon and Fine, 1996; Talley, 2013). The ITF plays important roles in not only heat and salt balance of both the Pacific and Indian oceans, but also the global climate (Gordon, 2005). The water transport, i.e., volume, heat, and salt or freshwater transports, are one of the most fundamental issues for the ITF studies. The volume transport of the ITF is estimated at a low value of –1.7 Sv (1 Sv = $10^6$ $m^3/s$) by Wyrtki (1961) and much higher values from –5.1 Sv up to –18 Sv summarized by Gordon (1986) before direct measurements of current are available (negative value indicates volume transport from the Pacific to Indian Ocean). The heat transport of the ITF is estimated in the range of 0.24–1.15 PW (1 PW = $10^{15}$ W) from the Pacific to Indian Ocean (Hirst and Godfrey, 1993; Tillinger and Gordon, 2010; Xie et al., 2019; Zhang et al., 2019). In addition to the ITF, there is a South China Sea branch of the cross-basin water transport route, with observed volume, heat, and freshwater transport of (–0.78 ± 0.12) Sv, (–77.31 ± 4.99) TW (1 TW = $10^{12}$ W), and (–30.87 ± 6.15) mSv (1 mSv = $10^{-3}$ Sv) from the South China Sea to the Indonesian seas through the Karimata Strait, which in turn join the main route of the ITF in the south of Makassar Strait (Fang et al., 2010; Susanto et al., 2013; Wang et al., 2019; Wei et al., 2019; Xu et al., 2021). There is no direct measurement of freshwater transport of the ITF been reported yet.

Since 1983, repeated expendable bathythermography (XBT) have been launched along the section between Fremantle, Australia and Sunda Strait, Indonesian (IX1 section) to measure up-

Foundation item: The Fund of Laoshan Laboratory under contract No. LSKJ202202700; the National Natural Science Foundation of China under contract Nos 42076023, 42076024 and 41876027; the Global Change and Air-Sea Interaction II Project under contract No. GASI-01-AIP-STwin.

*Corresponding author, E-mail: weizx@fio.org.cn

per ocean temperature and monitor the ITF variability. Using the temperature of XBT operation along the IX1 section, Meyers et al. (1995) gave an estimation of 5 Sv for the ITF geostrophic transport relative to 400 m water depth. The ITF geostrophic transport across the IX1 section has been updated by subsequent studies, showing large uncertainty caused by the different assumption of salinity (Liu et al., 2005, 2015; Wijffels et al., 2008). Satellite altimeter observation provides another method for the ITF transport proxy by empirical formula, to produce a longer time series to study the interannual variability of the ITF (Potemra, 2005; Sprintall and Révelard, 2014; Susanto and Song, 2015).

Direct measurements of the ITF transport come from the International Nusantara Stratification and Transport (INSTANT) program from 2004 to 2006 (Sprintall et al., 2004, 2009; Gordon et al., 2010) and earlier Arlindo program from 1996 to 1998 (Gordon et al., 1999; Susanto and Gordon, 2005). When the INSTANT program ended in 2006, a single mooring in the Makassar Strait was maintained to date (monitoring the ITF, MITF) (Susanto et al., 2012; Gordon et al., 2019). Gordon et al. (2019) summarized the longterm direct measurement of current velocity profiles in the Makassar Strait covering the Arlindo, INSTANT and MITF periods from December 1996 to August 2017. Their results show longterm mean Makassar Strait throughflow transport of about 12–13 Sv, approximately 77% of the total ITF transport, with multi-time scale variations from intraseasonal to seasonal, interannual and decadal, which are associated with the intraseasonal Kelvin waves (Pujiana et al., 2013; Napitu et al., 2019; Pujiana and McPhaden, 2020), monsoon (Susanto et al., 2012), Indian Ocean Dipole (IOD) and El Niño3.4-Southern Oscillation (ENSO) (Sprintall and Révelard, 2014; van Sebille et al., 2014; Yuan et al., 2013; Pujiana et al., 2019), and Interdecadal Pacific Oscillation (IPO) (Li et al., 2020).

As the ITF is dynamically driven by the Pacific-Indian pressure head that determined by large scale distribution of the Indo-Pacific wind (Wyrtki, 1987), ocean circulation models generally could reproduce a reasonable annual mean total ITF transport (Du and Qu, 2010; Lee et al., 2010; Metzger et al., 2010). However, there are rarely ocean models could reproduce appropriate ITF details, e.g., semi-annual phase, intraseasonal and interannual variabilities, and transport proportion in different straits/passages (Humphries and Webb, 2008; Tillinger and Gordon, 2009; Metzger et al., 2010; Zhao et al., 2015; Liang et al., 2019). These deficiencies are attribute to complex topography, strong mixing, frequent internal waves, and active air-sea interactions in the ITF regions (Sprintall et al., 2019). Insufficient data assimilation in the ITF region may also a limitation for improved ITF simulation. The Simple Ocean Data Assimilation (SODA) has released its version 3 dataset, with different ensemble members that forced by various surface forcings, providing opportunity for comparing the simulated ITF in a same ocean model configuration (Carton et al., 2018). Therefore, in this study, we will focus on the consistency and discrepancy among the SODA3 ensemble members in simulating the ITF in Makassar Strait, where the long-term time series of *in situ* observed current velocity profiles are available. The ITF in the Lombok and Ombai straits are not considered because the two straits are not well resolved in the SODA3 products. We do not analyse outside ocean reanalysis because they are produced based on another ocean model configuration, thereby certainly leading to different ITF characteristic.

The remainder of this paper is organized as follows: Section 2 describes the direct measurement of current profiles in the Makassar Strait and the SODA3 dataset, and introduces the analysis methods. Sections 3–6 compare the simulated ITF in the Makassar Strait across the SODA3 ensemble members with the observations and other reanalysis dataset. Section 7 gives the discussion and conclusions.

## 2 Data and methods

### 2.1 *Direct measurement of the Indonesian Throughflow*

The direct measurements of the ITF in the Makassar Strait are obtained from Gordon et al. (2019). In this study, we use the current velocity profiles observed by moorings during the INSTANT (January 2004 to November 2006) and MITF (November 2006 to August 2017) periods. The INSTANT moorings were deployed at Mak-West (2°51.9′S, 118°27.3′E) and Mak-East (2°51.5′S, 118°37.7′E) (Fig. 1). Both moorings were equipped with an upward-looking and a downward-looking RD Instruments 75 kHz Acoustic Doppler Current Profilers (ADCP) at a nominal depth of 300 m, and single point current meters at 400 m and 750 m. The Mak-West mooring was equipped with two additional current meters at 200 m and 1 500 m. The MITF maintains the Mak-West mooring, with slight changes in mooring configuration of the nominal depths of the instruments for the periods of 2007–2009, 2009–2011, and 2011–2017. These observed zonal and meridional velocities are compiled with a vertical resolution of 20 m from 40–760 m and hourly time interval, covering the periods from January 18, 2004 to August 18, 2017 (missing data from August 2011 to August 2013), and can be downloaded from https://www.ldeo.columbia.edu/~bhuber/MITF/.

### 2.2 *Satellite derived sea surface wind product*

The sea surface winds at 10 m are from the Cross Calibrated Multi-Plantform (CCMP) Version 2.0 with a horizontal resolution of 0.25° × 0.25° and time interval of 6 hours, covering the period of 1987 to 2019. The CCMP version 2.0 is produced by Remote Sensing Systems based on consistently cross-calibrated satellite winds (i.e., scatterometers QuikScat and ASCAT-A as well as the SSM/I, SSMIS, TMI, GMI, ASMR-E, AMSR2, and WindSat radiometers), *in situ* measurements from moored buoys, and background winds from the ERA-Interim reanalysis (Atlas et al., 2011; Mears et al., 2019).

### 2.3 *SODA3 reanalysis products*

The SODA3 was designed to reconstruct the historical simulation of the ocean dynamical environment, based on ocean numerical models with assimilation of available observations (Carton et al., 2018). The SODA3 is built on the Modular Ocean Model, version 5 (MOM5), with 1 440×1 070 eddy permitting quasi-isotropic horizontal grid cells (zonally 0.25° and meridionally varying from 0.1° at high latitude to 0.25° in tropics), and 50 vertical levels on an Arakawa B-grid (Delworth et al., 2012). The ingested observations include the World Ocean Database of historical hydrographic profiles (Boyer et al., 2013), and *in situ* and remote sensing sea surface temperature (SST) from the International Comprehensive Ocean-Atmosphere Data Set (ICOADS) version 5 (Woodruff et al., 2011) and the L3 Pathfinder version 5.2 Advanced Very High Resolution Radiometer (AVHRR) (Casey et al., 2010). The SODA3 releases a series of reanalysis ensemble members with different forcing and bulk formula. The Modern-Era Retrospective Analysis for Research and Applications, Version 2 (MERRA2) is an atmospheric reanalysis of the modern satellite era produced by NASA's Global Modeling and Assimilation Office (GMAO) (Gelaro et al., 2017). ERA-Interim is a global atmospheric reanalysis produced by the European Centre for Medium-Range Weather Forecasts (ECMWF) (Dee et al., 2011).

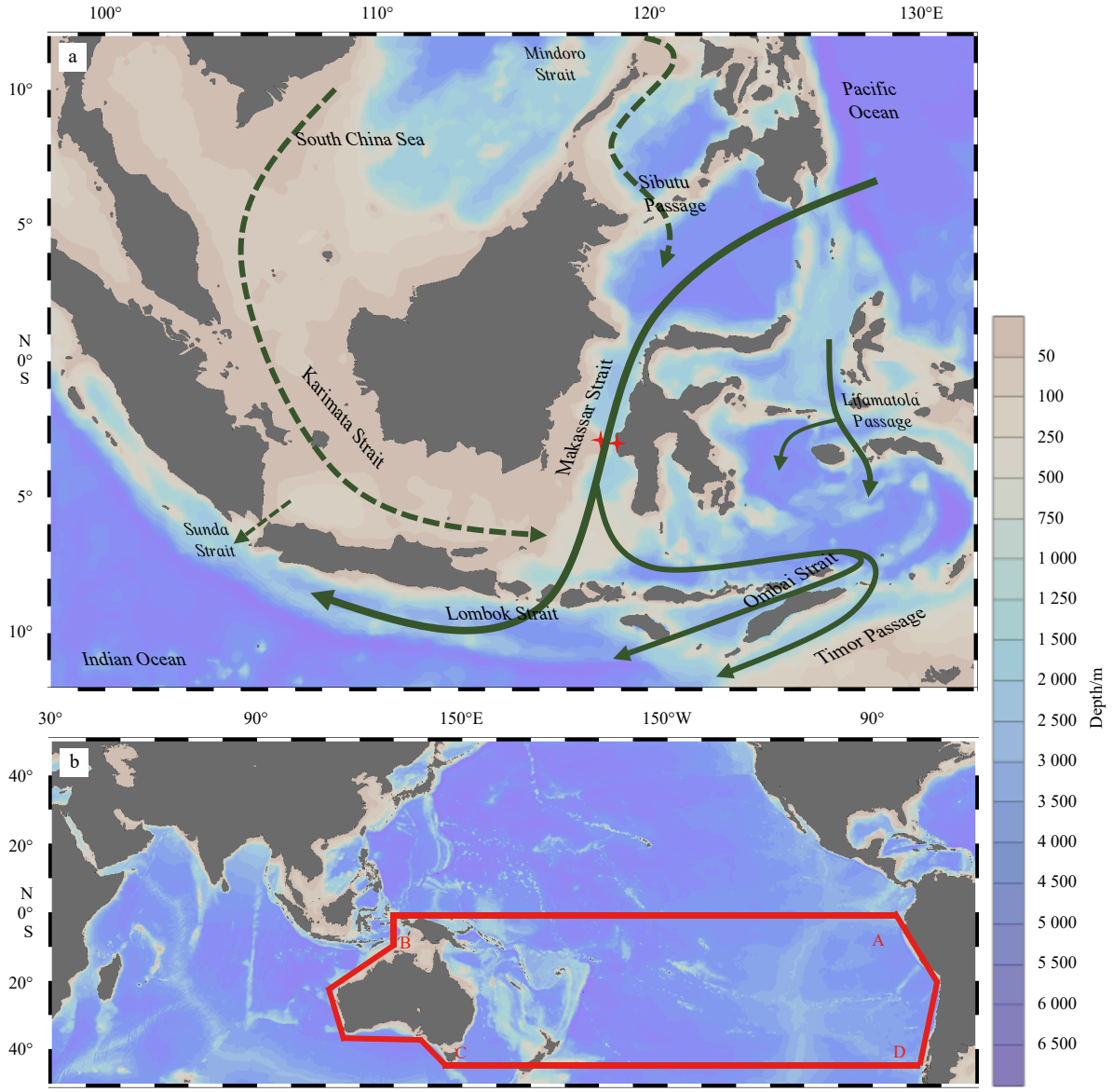


**Fig. 1.** The sketch map of the Indonesian Throughflow (solid arrows) and the South China Sea branch (dashed arrows) of the Pacific to Indian Ocean Throughflow (following Fang et al. (2010)) (a), with red stars in donating the subsurface mooring stations of Mak-West (2°51.9′S, 118°27.3′E) and Mak-East (2°51.5′S, 118°37.7′E) during the INSTANT and MITF periods, and the integration route for the wind stress in the Island Rule calculation (red lines) (b).

The Coordinated Ocean Research Experiments version 2 (COREv2) provides a set of common atmospheric boundary conditions to force ocean models and has been widely used, sponsored by the CLIVAR Working Group for Ocean Model Development (WGOMD) (Large and Yeager, 2009; Griffies et al., 2009). The Japanese 55-year Reanalysis (JRA-55) is a homogeneous climate dataset with sophisticated data assimulation, produced by the Japan Meteorological Agency (JMA) (Kobayashi et al., 2015; Harada et al., 2016). The Drakkar Forcing Set 5.2 (DFS5.2) was developed to drive ocean hindcasts based on ERA-interim reanalysis (Dussin et al., 2016). The JRA-55DO is a surface dataset based on the JRA-55 (Tsujino et al., 2018), and is used to drive ocean-sea ice models that involved in the Phase 2 of the Ocean Model Intercomparison Project (OMIP-2). The Large-Yeager (Large and Yeager, 2004, 2009) and COARE4 (Fairall et al., 2003) bulk formulas optional employed in different ensemble members of SODA3. Of these reanalysis datasets, they were remapped onto a 0.5° × 0.5° horizontal grid with 50 vertical levels from the native grid (Carton et al., 2018). In this study, we analyse nine of the SODA3 ensemble members with no data assimilation in SODA3.3.0 and optimum interpolation (OI) assimilation method in the rest (Table 1).

### 2.4 *Other ocean reanalysis products*

Two previous version of the SODA3 products, i.e., the SODA2.0.2 and SODA2.2.4, as well as 4 other ocean reanalysis products, are also used for intercomparison. The SODA2.0.2 and SODA2.2.4 are developed based on the Parallel Ocean Program (POP) ocean model, with a horizontal resolution of 0.5° × 0.5° and 40 vertical levels, covering the period of 1958–2001 and 1871–2010, respectively (Carton and Giese, 2008). The ocean analysis/reanalysis system (ORA-S3 and ORAS4) are implemented by

**Table 1.** Details of the SODA3 reanalysis products used in the present study

| No. | Dataset | Assimilation | Forcing | Forcing resolution | Bulk formula | Period |
|---|---|---|---|---|---|---|
| 1 | SODA3.3.0 | no assimulation | MERRA2 | ~0.5° × 0.625° | Large-Yeager | 1980–2015 |
| 2 | SODA3.3.1 | optimum interpolation | MERRA2 | ~0.5° × 0.625° | Large-Yeager | 1980–2015 |
| 3 | SODA3.3.2 | optimum interpolation | MERRA2 | ~0.5° × 0.625° | COARE4 | 1980–2017 |
| 4 | SODA3.4.1 | optimum interpolation | ERA-Interim | ~80 km (T255) | Large-Yeager | 1980–2016 |
| 5 | SODA3.4.2 | optimum interpolation | ERA-Interim | ~80 km (T255) | COARE4 | 1980–2017 |
| 6 | SODA3.6.1 | optimum interpolation | COREv2 | 1° × 1° | Large-Yeager | 1980–2009 |
| 7 | SODA3.7.2 | optimum interpolation | JRA-55 | ~55 km (TL319) | COARE4 | 1980–2016 |
| 8 | SODA3.11.2 | optimum interpolation | DFS5.2 | ~0.7° × 0.625° | COARE4 | 1980–2015 |
| 9 | SODA3.12.2 | optimum interpolation | JRA-55DO | ~55 km (TL319) | COARE4 | 1980–2016 |

the ECMWF. The ORA-S3 is on a horizontal resolution of 1° × 1° at 29 vertical levels from 1959 to 2011 (Balmaseda et al., 2008). The ORAS4 is on a horizontal resolution of 1° × 1° at 42 vertical levels from 1958 to 2013 (Balmaseda et al., 2013). The GLBa0.08 dataset of the Hybrid Coordinate Ocean Model (HYCOM) products, with a horizontal resolution of (1/12)° × (1/12)° at 33 vertical levels from 2004 to 2014, are also used (Bleck and Boudra, 1981).

### 2.5 *Methods*

Based on the steady and frictionless Sverdrup theory, the ITF transport ($F_{IR}$) can be estimated by the Island Rule (Godfrey, 1989):

$$F_{IR} = \frac{1}{f_N - f_S} \oint \frac{\tau}{\rho_0} \mathrm{d}l, \tag{1}$$

where $f_N$ and $f_S$ are the Coriolis parameter at the southern (~44°S) and northern (0°) legs of the integration route, respectively. $\rho_0$ is the averaged density of ocean, taken as 1 035 kg/m$^3$. $\tau$ is the along route wind stress, which is integrated along the enclosed route as marked by red lines in Fig. 1.

The ITF volume transport ($F_v$) in Makassar Strait is calculated as the area integral of the normal velocity across the transect (3°S, 116°–119°E), as follows:

$$F_v = \int_A v \mathrm{d}A, \tag{2}$$

where $v$ is the meridional velocity across the transect, and d$A$ donates the area element.

Heat transport ($F_H$) and freshwater transport ($F_W$) is calculated as follows:

$$F_H = \rho C_p \int_A (T - T_0)\, v \mathrm{d}A, \tag{3}$$

$$F_W = \rho \int_A \left[\frac{S_0 - S}{S_0}\right] v \mathrm{d}A, \tag{4}$$

where $\rho$, $T$, and $S$ are the sea water density, temperature and salinity in the transect, respectively; $C_p$ is the specific heat (3.89 × 10$^3$ J/ (kg·℃)); and $T_0$ and $S_0$ are the reference temperature and salinity, set to 3.72℃ and 34.62, as suggested by previous studies (Schiller et al., 1998; Fang et al., 2010; Xu et al., 2021).

The Niño3.4 index is defined as the averaged SSTA in the area of the equatorial central and eastern Pacific (5°S–5°N, 170°–120°W). The Dipole Mode Index (DMI) is calculated as the difference of SSTA between the western (10°S–10°N, 50°–70°E) and southeastern tropical Indian Ocean (10°S–0°, 90°–110°E) (Saji et al., 1999).

## 3 Comparison with observed ITF in the Makassar Strait

During the INSTANT and MITF periods, the mooring observed velocity profile shows vertically increasing of southward velocity in the upper layer and then deceasing with depth, with maximum value of approximately –0.63 m/s occurring within the 100 m to 120 m depth interval (Fig. 2a). The vertical structure of subsurface velocity maximum is well reproduced by the SODA3 datasets, with ensemble mean value of (–0.75 ± 0.16) m/s at 120 m depth (Fig. 2a). The temperature profiles in the Makassar Strait are vertically consistently distributed among the SODA3 datasets, with standard deviations from 0.01℃ to 0.36℃, generally smaller than 2% of the multi-dataset ensemble means temperature (Fig. 2b). Note that the simulated temperature shows larger biases up to 5.39℃ in the mixed and thermocline layers, and smaller biases only around 0.08℃ beneath the 300 m depth (Fig. 2b). In observation, the salinity maximum (34.64) co-occurs with the velocity maximum, suggesting intrusion of the North Pacific Subtropical Water (NPSW); a salinity minimum core (34.05) at around 300 m, with temperature of 10℃ and velocity of –0.34 m/s, suggesting the intrusion of the North Pacific Intermediate Water (NPIW) (Gordon and Fine, 1996; Ilahude and Gordon, 1996). In comparison, the salinity maximum core (34.80 ± 0.13) is at the same depth range of the velocity maximum, i.e., 120 m depth on average in the SODA3 dataset, which is deeper and saltier than

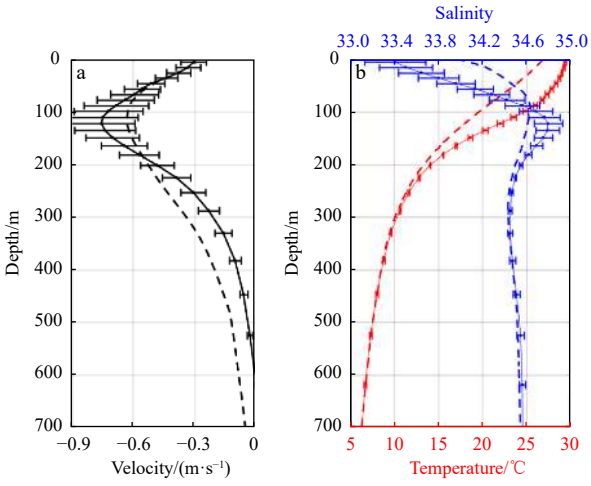


**Fig. 2.** The multi-dataset ensemble means of SODA3 (solid lines) and observed (dashed lines) velocity and temperature/salinity profiles in the Makassar Strait. a. Along-strait velocity; b. temperature (red lines) and salinity (blue lines). The error-bars indicate the standard deviation of the SODA3 products.

that in observation (Fig. 2b). The simulated salinity minimum that associated with NPIW is in good agreement with the observation (Fig. 2b). Meanwhile, the SODA3 dataset tend to produce lower salinity in the upper 100 m, with underestimated biases around 0.07–0.73.

The temperature-salinity ($T$-$S$) diagrams in the Makassar Strait in the SODA3 ensemble members are shown in Fig. 3. Both data assimilation and the bulk formulas could result in different thermohaline structures in the Makassar Strait as derived from the SODA3 ensemble members. The non-assimilated SODA3.3.0 produces the NPSW with higher salinity (~35.15) than those with data assimilation (~34.73–34.78), both are higher than the observation (~34.64). On the contrary, the NPIW is of lower salinity (~34.36) in SODA3.3.0 than others (~34.47) and the observation (~34.05). The NPSW and NPIW are consistently identified as between the isopycnal surfaces $\sigma_\theta$ of 23–25, and 26–27, respectively. There are wider ranges of salinity for surface waters in SODA3.3.0, SODA3.3.2, SODA3.4.2, SODA3.7.2, SODA3.11.2, SODA3.12.2 than SODA3.3.1 and SODA3.4.1, which may attribute to different Bulk formula, i.e., Large-Yeager in the former and COARE4 in the later ensemble members.

The simulated annual cycles of the along strait velocity through the Makassar Strait are compared with observations (Fig. 4). In observation (Fig. 4a), the along strait velocity shows intensified subsurface velocity maximum exceeding –0.8 m/s during the boreal summer (July to September). The subsurface velocity maximums are getting weaker from November to January, with speed values approximately of –0.5 m/s, and at a much deeper depth of near 150 m, compared with 70–120 m during boreal summer. There are northward flows at the intermediate depth in May and November, which are induced by the propagation of semi-annual Kelvin waves, with averaged upward propagating phase from 700 m to 200 m of approximately 44.7 m/s and 23.3 m/s for the May and November events, respectively, in agreement with previous investigation of Susanto et al. (2012).

In the SODA3 ensemble members, they generally have reproduced that the occurrence of velocity maximum at the subsurface layer. However, the simulated ensemble mean ITF in the Makassar Strait is stronger by up to 0.2 m/s in the upper 150 m, and weaker by more than 0.2 m/s between around 200–700 m, with the largest bias cores at around 70–100 m from March to May, and from September to December, and around 300–450 m from January to February, respectively (Fig. 4a). In addition, the simulated ITF in the Makassar Strait is weaker than observation by up to 0.3 m/s in the upper 700 m in SODA3.3.0 and SODA3.3.1, with larger biases in the subsurface layer of 70–100 m, and 200–450 m (Figs 4b and c). In the rest ensemble members of SODA3, there are consistently stronger and weaker flows in the upper 200 m and 250–700 m, respectively (Figs 4d–j). The SODA3 datasets may partly capture the observed annual cycle features of stronger/weaker throughflow during boreal summer/winter, and semi-annual variability that associated with the propagation of

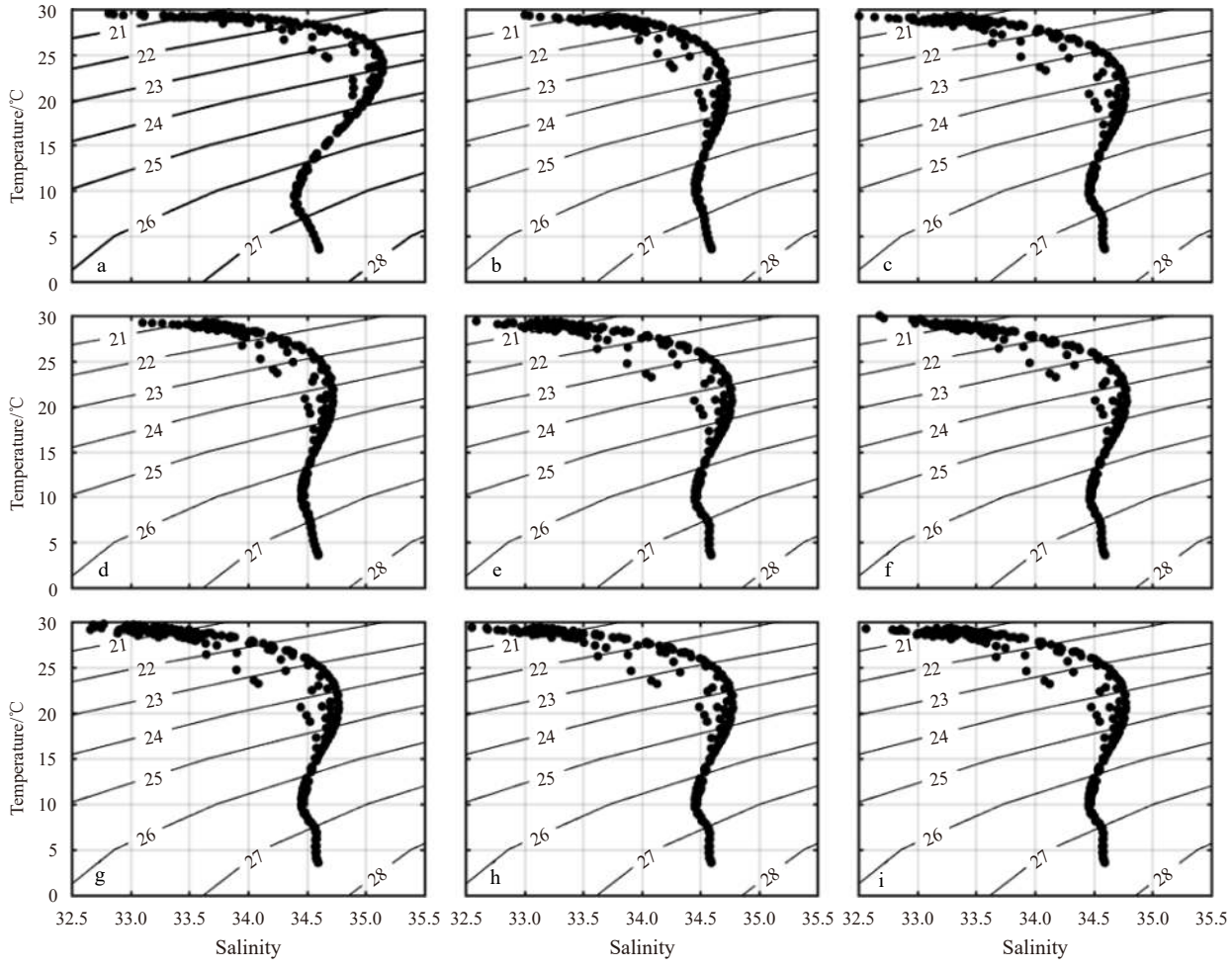


**Fig. 3.** $T$-$S$ diagram in the Makassar Strait. a. SODA3.3.0, b. SODA3.3.1, c. SODA3.3.2, d. SODA3.4.1, e. SODA3.4.2, f. SODA3.6.1, g. SODA3.7.2, h. SODA3.11.2, and i. SODA3.12.2.

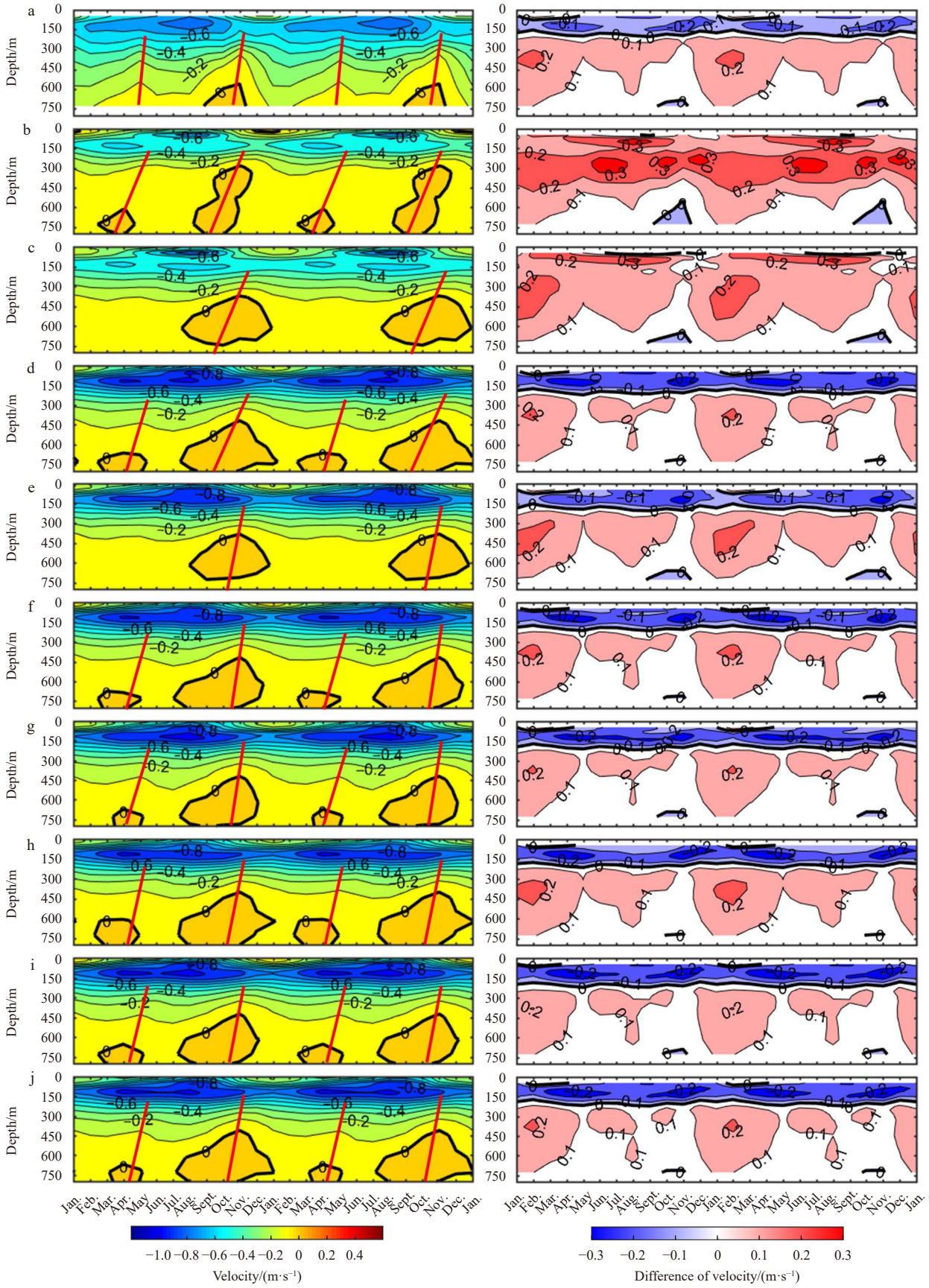


**Fig. 4.** The annual cycle of the along strait velocity in the Makassar Strait (left column) and the differences between the SODA3 and observation (right column). a. Observation and differences between SODA3 ensemble mean and observation; b–j. different SODA3 ensemble members as listed in Table 1. Red lines in the left column indicate the phase lines of the semi-annual Kelvin waves.

semi-annual Kelvin waves. In terms of the semi-annual variability, it appears as upward propagating phase with speeds of 8.5–15.9 m/d and 8.5–23.2 m/d for the May and November events, respectively, slower than in observation (Figs 4b–j). In most of the ensemble members, the phase speeds are slower in May than in November, in contrast with the observation. The semi-annual Kelvin waves in May are not well identified in SODA3.3.1 and SODA3.4.1 datasets (Figs 4c and e).

The along strait velocity in Makassar Strait shows weaker interannual variability than observation in the non-data assimilated SODA3.3.0, with amplitude generally near 0.1 m/s, compared with as large as 0.3 m/s in the observation (Figs 5a and b). In contrast, the ensemble members with data assimilation, have produced stronger interannual variability in the Makassar along strait velocity with opposite anomalies between the depth layers above and below around 300 m or so (Figs 5c–j). The simulated

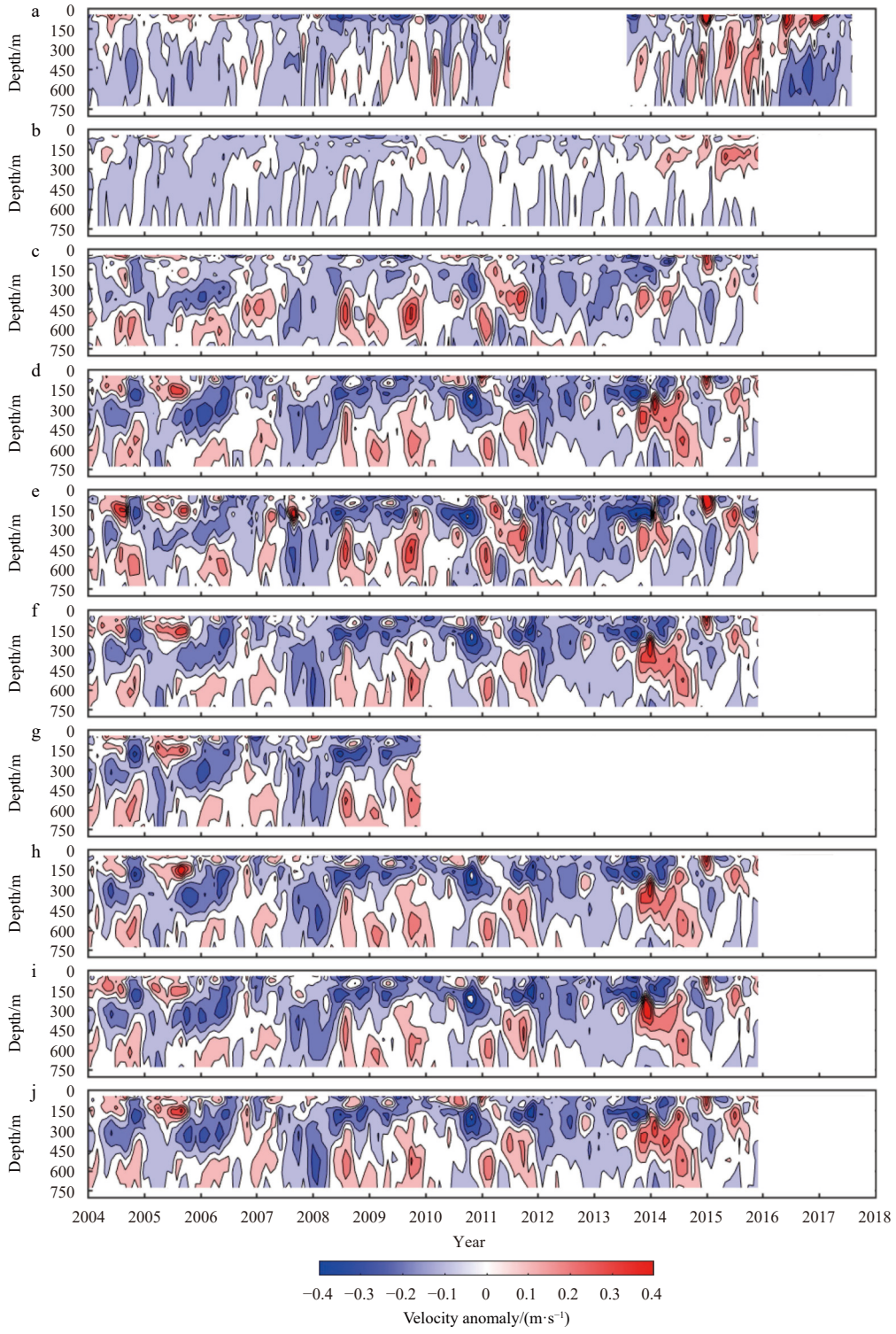


**Fig. 5.** The along strait velocity anomalies in the Makassar Strait. a. Observation, b. SODA3.3.0, c. SODA3.3.1, d. SODA3.3.2, e. SODA3.4.1, f. SODA3.4.2, g. SODA3.6.1, h. SODA3.7.2, i. SODA3.11.2, and j. SODA3.12.2.

strong/weak Makassar throughflow years are generally coincide with the observation, albeit with slightly differences in phases and vertical structures. For example, there are consistently increased and decreased southward flow during the persistent La Niña (2008–2010) and El Niño (2014–2016) conditions.

## 4 Volume, heat and freshwater transport through the Makassar Strait

The annual mean volume transports in the Makassar Strait calculated from the along strait velocity (upper 700 m) and the Island Rule (based on CCMP Version 2.0 wind data) are (−12.50 ± 2.83) Sv and (−12.22 ± 1.78) Sv, respectively (Fig. 6a). In comparison, the SODA3.3.0 and SODA3.3.1, forced by MERRA2 and Large-Yeager bulk formula, yield to smaller annual mean volume transports of (−7.24 ± 1.06) Sv and (−9.23 ± 1.29) Sv using along strait velocity (upper 728 m), and (−9.84 ± 1.19) Sv and (−10 ± 1.19) Sv based on Island Rule, respectively (Fig. 6a). In SODA3.3.2, forced by MERRA2 but with COARE4 bulk formula, it gives annual mean values of (−11.73 ± 1.35) Sv and (−12.14 ± 1.51) Sv based on along strait velocity (upper 728 m), respectively. The SODA3.4.1 and SODA3.4.2, forced by ERA-Interim with Large-Yeager and COARE4 bulk formulas, and SODA3.11.2, forced by DFS5.2 with COARE4 bulk formula, produce volume transport roughly equal to the SODA3.3.2 and observation, approximately of (−11.05 ± 1.46) Sv, (−11.39 ± 1.37) Sv, and (−11.88 ± 1.34) Sv, slightly smaller than estimated from the Island Rule, which are (−11.97 ± 1.52) Sv, (−12.55 ± 1.65) Sv, and (−12.54 ± 1.49) Sv, respectively. The SODA3.6.1, forced by COREv2 with Large-Yeager

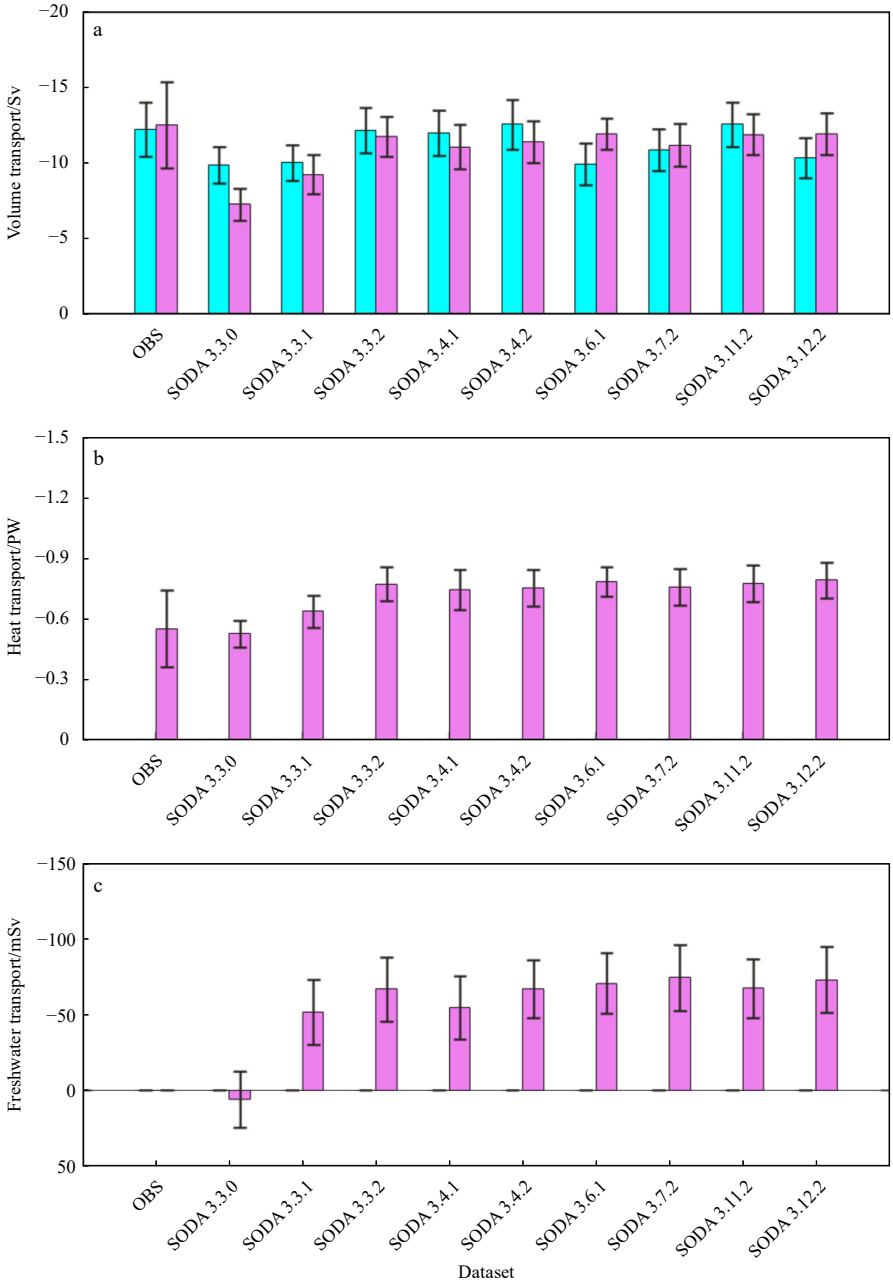


**Fig. 6.** Annual mean transport of volume (a), heat (b), and freshwater (c) through the upper 700 m of the Makassar Strait in observations and SODA3 ensemble members. The cyan and pink bars in a are derived from the Island Rule and along strait velocity, respectively. Error bars indicate the standard deviation of the monthly transport time series.

formula, SODA3.7.2 and SODA3.12.2, forced by JRA-55 and JRA-55DO with COARE4 formula, produce volume transport roughly equal to the observation and the above mentioned SODA3 ensemble member except for SODA3.3.0 and SODA3.3.1, with values of (−11.93 ± 1.03) Sv, ( −11.17 ± 1.4) Sv, and (−11.91 ± 1.4) Sv, respectively. The Island Rule estimated transports are smaller than calculated from along strait velocity in SODA3.6.1, SODA3.7.2 and SODA3.12.2, with values of (−9.93 ± 1.39) Sv, (−10.83 ± 1.37) Sv, and (−10.3 ± 1.32) Sv, which are smaller than that based on CCMP version 2.0 sea surface wind. The observed heat transport through the Makassar Strait is (−0.55 ± 0.19) PW (Fig. 6b). In the SODA3 datasets, the heat transport is smaller in SODA3.3.0 (−0.52 ± 0.07) PW, whereas greater in others, i.e., ranging from (−0.64 ± 0.08) PW to (−0.79 ± 0.09) PW than in observation (Fig. 6b). There is no observed freshwater transport through the Makassar Strait. In the SODA3 datasets, the freshwater transport is (6.23±18.45) mSv (northward) in SODA3.3.0, and in a range of (−51.47 ± 21.62) mSv to (−74.27 ± 21.65) mSv in the rest SODA3 ensemble members (Fig. 6c). The SODA3.3.1 and SODA3.4.1 give the smallest, and SODA3.7.2 and SODA3.12.2 give the largest southward freshwater transports.

The annual cycle of the Makassar Strait transport is shown in Fig. 7. The vertical distribution of volume transport basically is reminiscent of the along strait velocity, showing intensified throughflow during boreal summer and northward transport in the intermediate depth of around 500–700 m in boreal fall (Fig. 7a). The standard deviations of the volume transport in the SODA3 ensemble members are generally one order smaller than the ensemble means values, with largest standard deviations occurring in the mixed layer during August to September, in the subsurface layer of 100–150 m during March to November (Fig. 7a). The heat transport is mainly contributed by the upper layer transport, and is intensified from May to October, with maximum values exceed −0.01 PW/m in the upper 75 m during boreal summer (Fig. 7b).

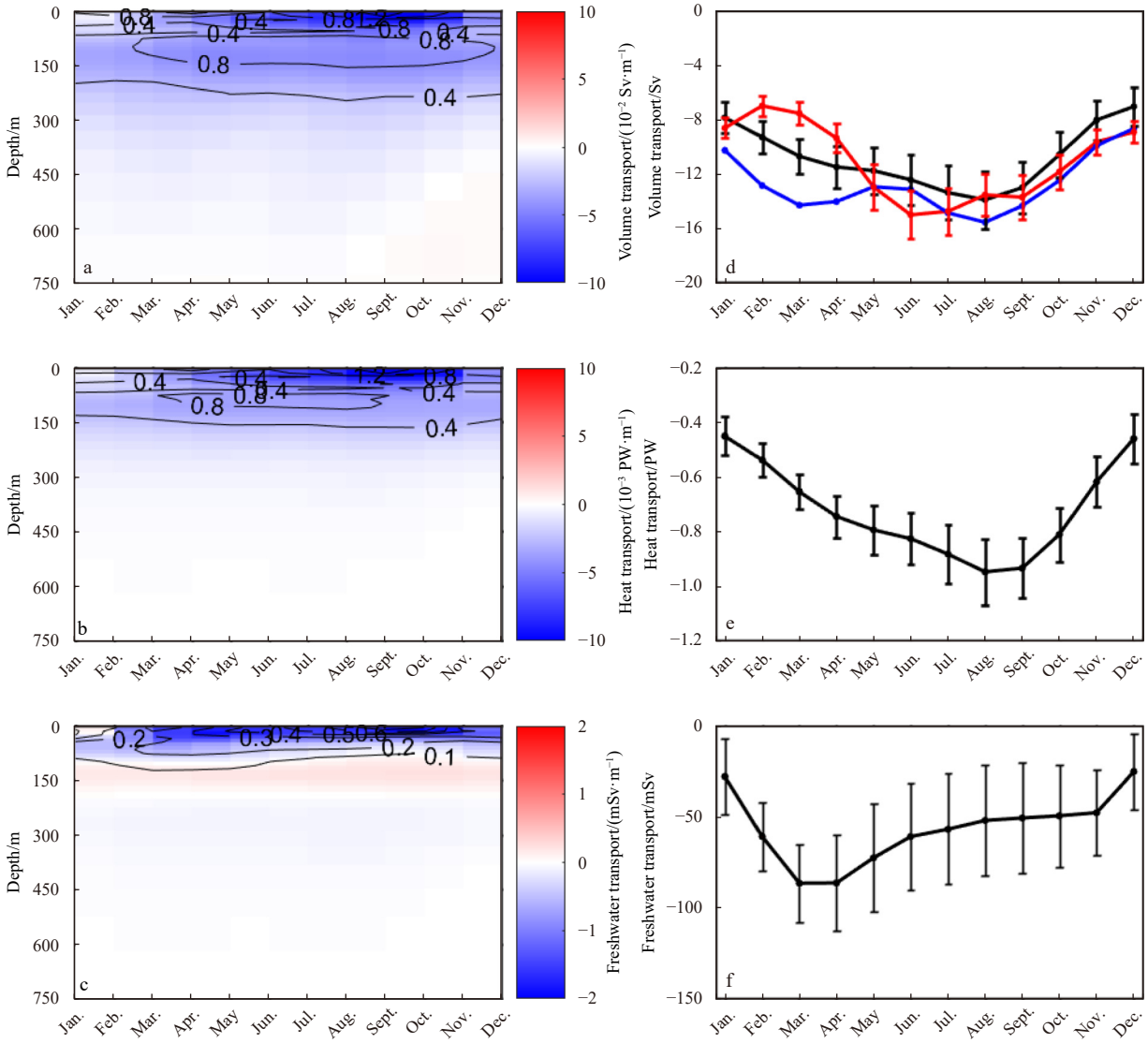


**Fig. 7.** Seasonal cycle of the volume (a), heat (b), and freshwater (c) transport per unit depth, and depth integrated volume (d), heat (e), and freshwater (f) transport in the upper 700 m through the Makassar Strait in SODA3 datasets. Shadings and contours in the left panels indicate the ensemble means and cross-ensemble member standard deviations of the SODA3 datasets. Solid black and red lines in d are calculated from the along strait velocity and Islands Rule based on SODA3 dataset, and blue line is from along strait velocity in observation. Error bars in d–f are the cross-ensemble member standard deviations of the SODA3 datasets. Unit: 1 Sv = $10^6$ $m^3/s$, 1 PW = $10^{15}$ W, 1 mSv = $10^{-3}$ Sv.

The cross-ensemble member standard deviations of heat transport are generally two order smaller than the ensemble means (Fig. 7b). The southward freshwater transport (negative values) in the Makassar Strait occurs in the upper mixed layer. Between the depth of around 100–200 m, the positive values suggest negative freshwater contribution of the ITF to the Indonesian seas, because there it carries high salinity NPSW in the subsurface (Fig. 7c). There is large uncertainty in terms of freshwater transport estimation in the SODA3 datasets, as revealed by that the standard deviations are nearly the same order with the ensemble means (Fig. 7c). The depth integrated volume, heat and freshwater transports are shown in Figs 7d–f. The seasonal cycle of the volume transport in the upper 700 m in SODA3 is basically in agreement with the observation, with maximum value of (–13.96 ± 2.10) Sv in August and minimum value of (–7.08 ± 1.40) Sv in December, respectively. The seasonal cycle of the heat transport in the upper 700 m is coincide with that of volume transport, approximately of (–0.95 ± 0.12) PW and (–0.45 ± 0.09) PW in August and December, respectively. In comparison, the freshwater transport reaches its maximum value of (–86.79 ± 21.62) mSv in March, and minimum value of (–25.46 ± 20.71) mSv in December. The seasonal cycle in freshwater transport is not in phase with the volume, which can be attribute to there are rainy season in boreal winter when there is smaller southward transport, whereas dry season in boreal summer when there is larger southward transport, in the Makassar Strait.

Figure 8 shows the vertical distribution of the interannual anomalies of volume, heat and freshwater transports in the SODA3 datasets. The interannual variability in volume transport generally shows enhanced southward transport (negative anomalies) occurred during the La Niña phases, i.e., 1984–1985, 1988–1989, 1999–2000, 2007–2008, and 2012–2013, and weaken southward transport (positive anomalies) occurred during the El Niño phases, i.e., 1986–1987, 1991–1992, 1994–1995, 1997–1998,

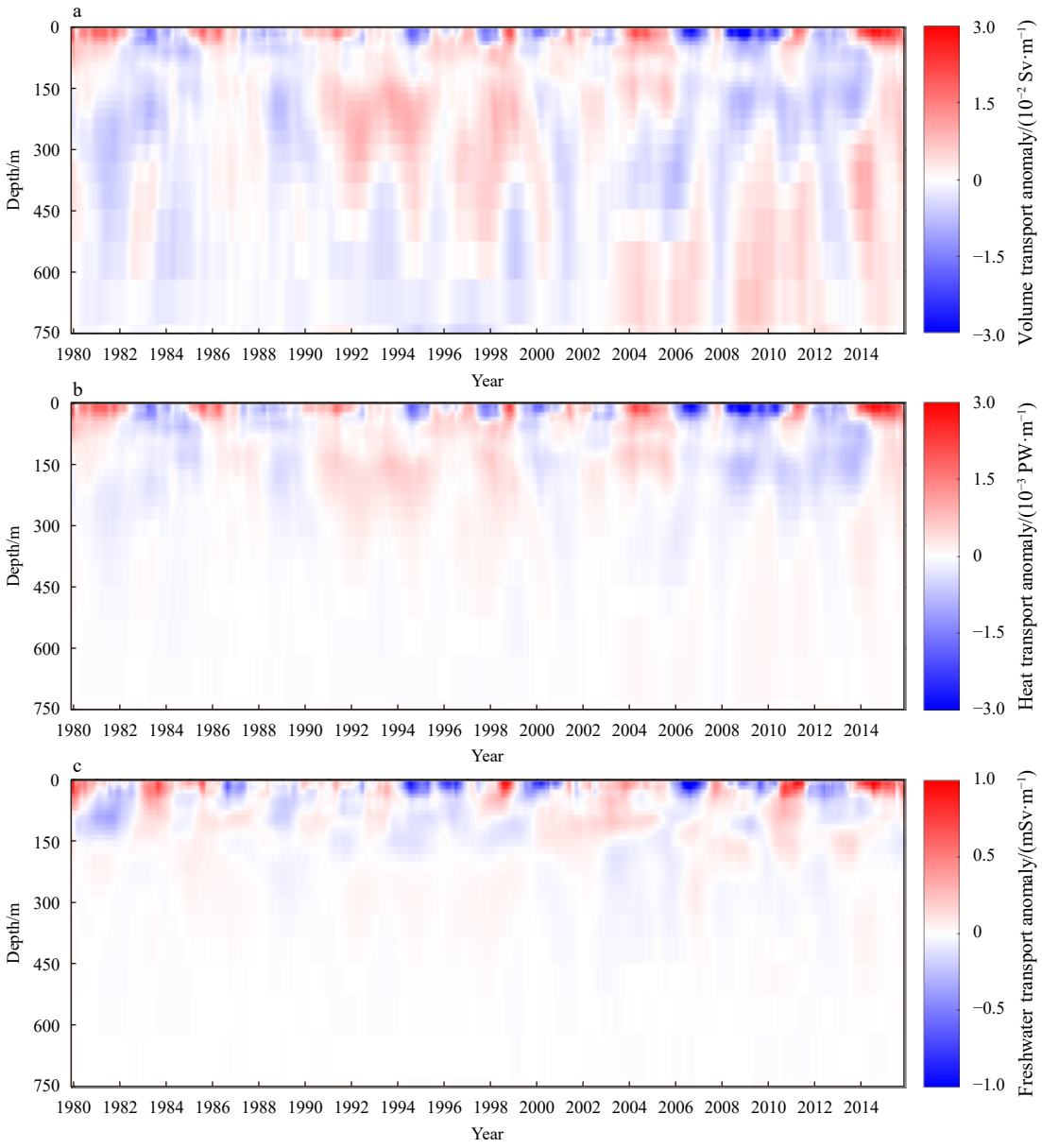


**Fig. 8.** Interannual anomalies of the volume (a), heat (b), and freshwater (c) transport per unit depth through the Makassar Strait in SODA3 datasets. Shadings and contours indicate the ensemble means and cross-ensemble member standard deviations of the SODA3 datasets. Unit: 1 Sv = 10 $^{6}$m$^{3}$/s, 1 PW = $10^{15}$ W, 1 mSv = $10^{-3}$ Sv.

2002–2003, and 2014–2015, respectively (Fig. 8a). The interannual variability in heat transport is basically coincide with that of volume transport in the Makassar Strait (Fig. 8b). The interannual variability in freshwater transport is not coincide with that in volume transport, and shows no preference with ENSO phases (Fig. 8c). This is somehow contradictory with the fact that there is more rainfall input to the Makassar Strait during La Niña years (Nur'utami and Hidayat, 2016; Hu and Sprintall, 2016), and thus favors enhanced southward freshwater transport as a result of the combination of fresher upper layer water and intensified throughflow in the Makassar Strait. This contradictory is probably due to artificially salinity simulation in the SODA3 dataset, especially for the non-assimilated SODA3.3.0.

## 5 Relationships with the IOD and ENSO

Figures 9–11 show the interannual anomalies of the depth integrated volume, heat and freshwater transports in the upper 700 m of the Makassar Strait and their lag correlations with the Niño3.4 and DMI indices in the SODA3 dataset. The simulated volume transport anomalies are in good consistent with the observation during 2004–2014 (Fig. 9a). The SODA3 identified ENSO and IOD events are basically corroborated with the observations (Figs 9a and c). The lag correlation between the volume transport anomalies and the Niño3.4 indices show significant positive correlation at time lags of –6 to 7 months, with peak value of 0.50 ± 0.07 at zero-time lag (Fig. 9b). There is no significant correlation between the Makassar volume transport anomalies and the DMI indices (Fig. 9c). The interannual variability in Makassar heat transport is in phase with that of volume transport, showing negative anomalies (enhanced heat transport) during the periods of 1982–1985, 1988–1989, 1999–2001, 2006–2010, and 2012–2013, and positive anomalies (weakened heat transport) during the periods of 1986–1987, 1990–1999, 2003–2005, 2011, and 2014–2015, respectively (Fig. 10a). The lag correlations of the heat transport anomalies with Niño3.4 and DMI indices show similar relationships with the volume transport (Figs 10b and c). The interannual variability in Makassar freshwater transport does not synchronous with the volume transport, i.e., showing negative anomalies (enhanced freshwater transport) during the periods of 1981–1982, 1988–1989, 1994–1996, 1999–2000, 2005–2006, 2009, and 2011–2012, and positive anomalies (weakened freshwater transport) during the periods of 1983–1984, 1985–1986, 1997–1998, 2001–2003, 2007–2008, 2010–2011, and 2013–2015, respectively (Fig. 11a). The interannual increase/decrease freshwater transport events occur with no preference of ENSO and IOD events (Figs 11a and c), which is also revealed by no significant lag correlations between the freshwater transport anomalies and the Niño3.4/DMI indices (Figs 11b and c).

Let the current and temperature in the Makassar Strait decomposing into seasonal cycles and anomalies $V = \overline{V} + V'$, and $T = \overline{T} + T'$, then the heat transport can be written as follows:

$$F_{\mathrm{H}} = C_p \rho \iint \left[ \left( \overline{T} - T_0 \right) \overline{V} + \left( \overline{T} - T_0 \right) V' + \overline{V} T' + T' V' \right] \mathrm{d}x\mathrm{d}z, \quad (5)$$

where the first through third terms of the right-hand side are the contributions from climatological state, velocity and temperature anomalies, respectively. The fourth term is higher order residual. As shown in Fig. 12, the seasonal variability contributes the largest variance, with mean value of (–0.71 ± 0.15) PW and

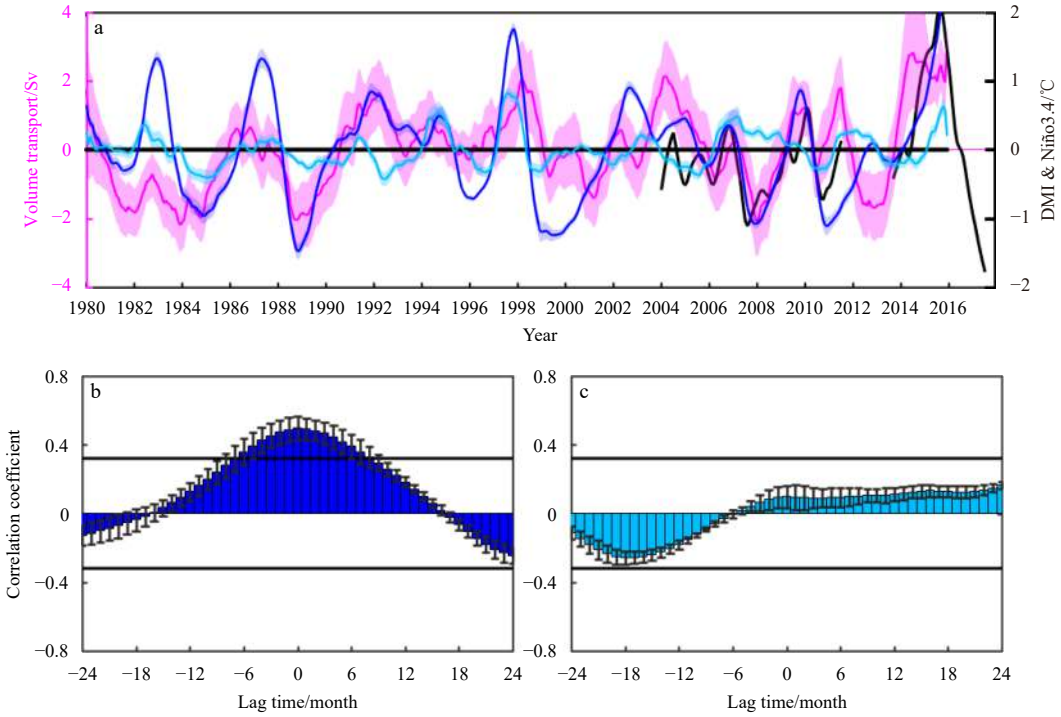


**Fig. 9.** Correlation analysis between the Makassar Strait volume transport and the Indo-Pacific climate modes. a. Interannual anomaly of volume transport through the Makassar Strait (magenta), the Dipole Mode Index (DMI) (cyan) and Niño3.4 index (blue). b and c. lag correlations of the Makassar Strait volume transport anomaly with Niño3.4 and DMI, with error bars indicate the cross-ensemble member standard deviations of the SODA3 datasets. The horizontal lines in b and c indicate the 95% significance level. Unit: 1 Sv = $10^6$ $m^3/s$.

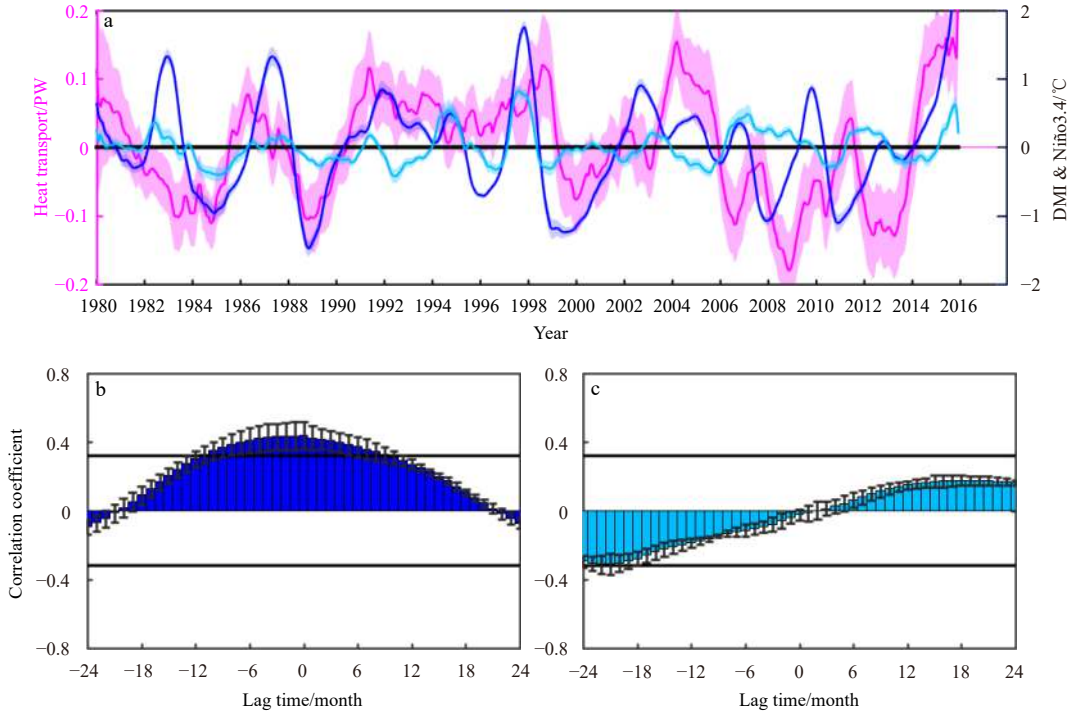


**Fig. 10.** Correlation analysis between the Makassar Strait heat transport and the Indo-Pacific climate modes. a. Interannual anomaly of heat transport through the Makassar Strait (magenta), the Dipole Mode Index (DMI) (cyan) and Niño3.4 index (blue). b and c. lag correlations of the Makassar Strait heat transport anomaly with Niño3.4 and DMI, with error bars indicate the cross-ensemble member standard deviations of the SODA3 datasets. The horizontal lines in b and c indicate the 95% significance level. Unit: 1 PW = $10^{15}$ W.

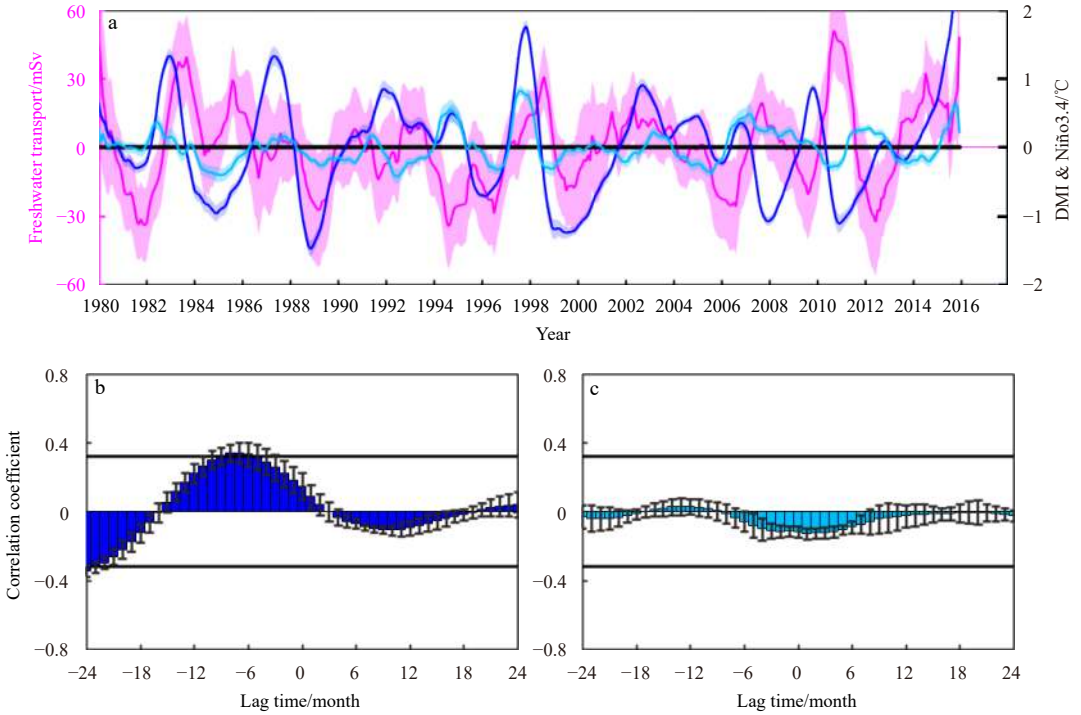


**Fig. 11.** Correlation analysis between the Makassar Strait freshwater transport and the Indo-Pacific climate modes. a. Interannual anomaly of freshwater transport through the Makassar Strait (magenta), the Dipole Mode Index (DMI) (cyan) and Niño3.4 index (blue). b and c. Lag correlations of the Makassar Strait freshwater transport anomaly with Niño3.4 and DMI, with error bars indicate the cross-ensemble member standard deviations of the SODA3 datasets. The horizontal lines in b and c indicate the 95% significance level. Unit: 1 mSv = $10^3$ $m^3/s$.

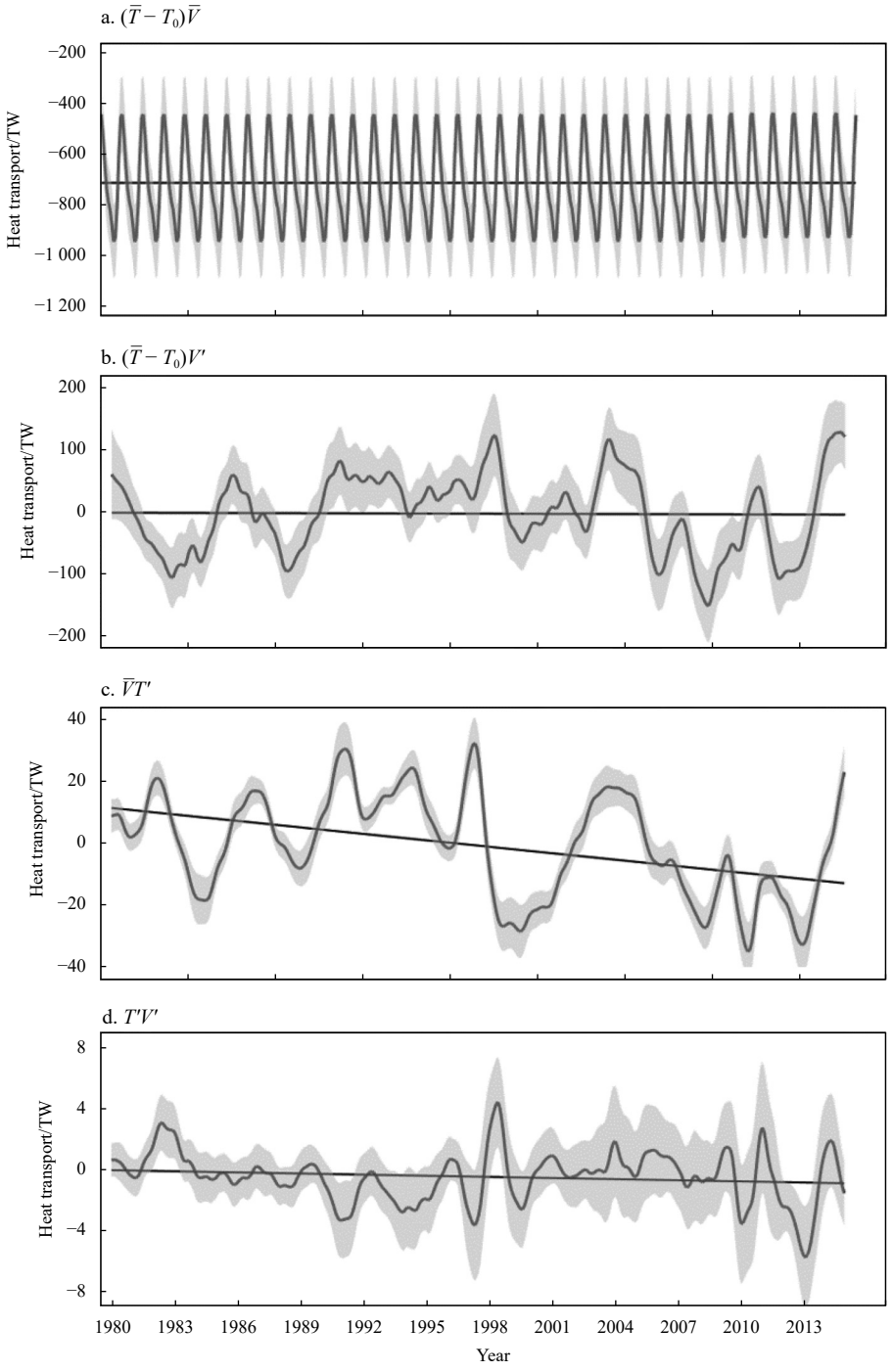


**Fig. 12.** Climatological mean state (a), velocity anomaly induced variation (b), temperature anomaly induced variation (c), and higher-order terms of the total heat transport through the Makassar Strait (d). Unit: 1 TW = $10^{12}$ W.

seasonal amplitude from (−0.44 ± 0.09) PW to (−0.94 ± 0.19) PW (Fig. 12a). The interannual variability in heat transport is associated with both the velocity and temperature anomalies, with correlation coefficients of 0.63 and 0.54, above the 95% confidence level, and accounting for approximately 87% and 8% of the interannual variation in the heat transport, respectively (Figs 12b and c). The temperature anomaly also explains a descending trend of approximately 0.7 TW/a, suggesting enhanced southward heat transport by ~25 TW over the period of 1980–2015 (Fig. 12c). The residual term shows a mean value of (−0.52 ± 2.24) TW and a maximum amplitude of (6.59 ± 1.24) TW (Fig. 12d).

Similarly, the freshwater transport in the Makassar Strait can be written as

$$F_{\mathrm{W}} = \iint \left[ \frac{(S_0 - S)\,\overline{V}}{S_0} + \frac{(S_0 - S)\,V'}{S_0} - \frac{S'\overline{V}}{S_0} - \frac{S'V'}{S_0} \right] \mathrm{d}x\mathrm{d}z, \quad (6)$$

where the first to third terms of the right-hand side represent the contributions from climatological state, velocity and salinity anomalies, respectively. As shown in Fig. 13, the seasonal variability contributes the largest variance, with mean value of (−58.64 ±

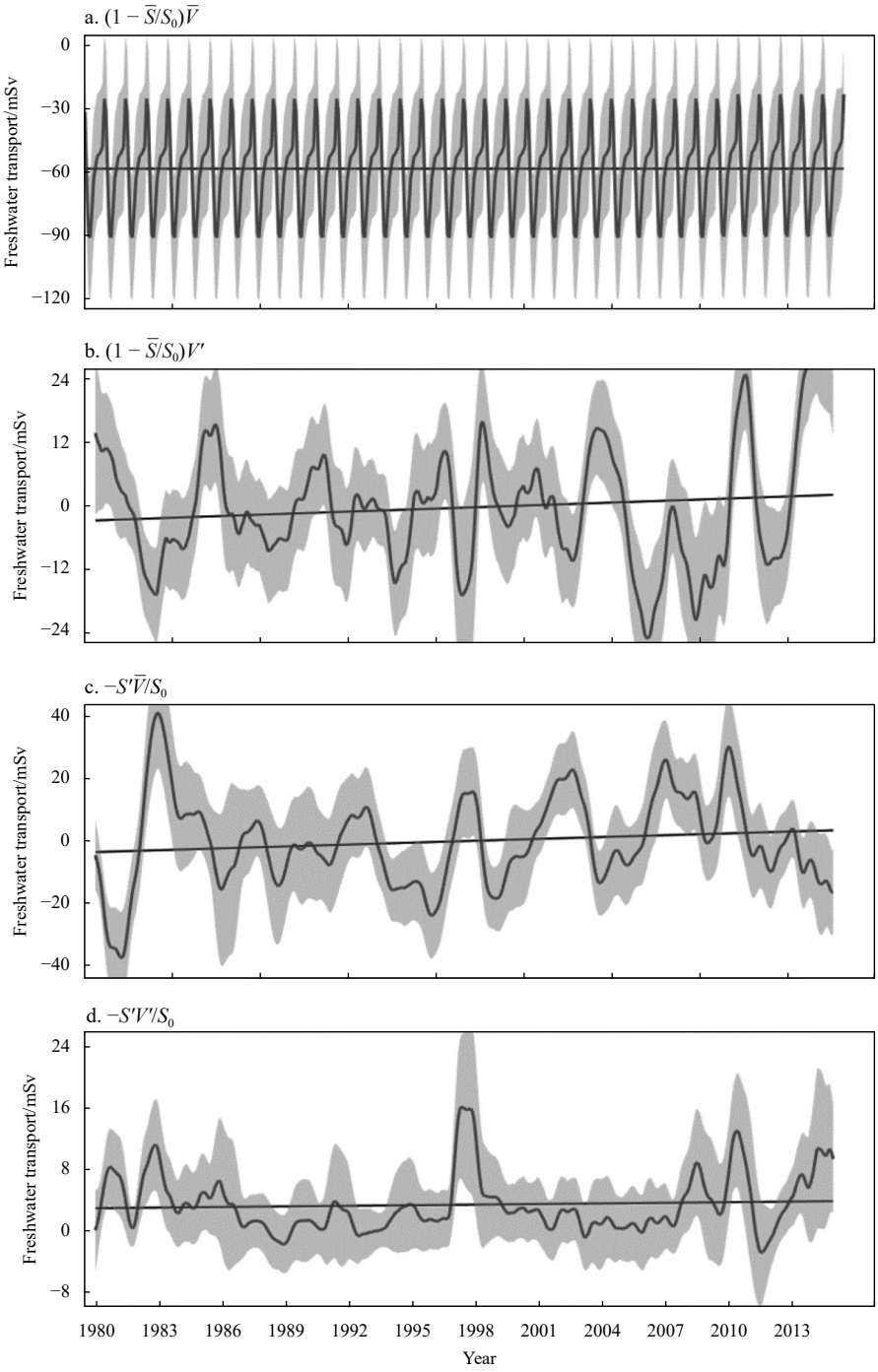


**Fig. 13.** Climatological mean state (a), velocity anomaly induced variation (b), salinity anomaly induced variation (c), and higher-order terms of the total freshwater transport (d) through the Makassar Strait. Unit: 1 mSv = $10^3$ $m^3/s$.

29.45) mSv and seasonal amplitude from (–23.53 ± 21.25) mSv to (–91.15 ± 35.75) mSv (Fig. 13a). The interannual variability in freshwater transport is associated with both the velocity and salinity anomalies, with correlation coefficients of 0.43 and 0.67, above the 95% confidence level, and accounting for approximately 41% and 56% of the interannual variation in the freshwater transport, respectively (Figs 12b and c). There are also weak ascending trends contributed by the velocity and salinity anomalies, approximately 0.22 mSv/a and 0.28 mSv/a, suggesting a total of weakened southward freshwater transport by 17.7 mSv over the period of 1980–2015 (Fig. 12c). The residual term shows a mean value of (3.33 ± 5.27) mSv and a maximum amplitude of (7.65 ± 7.35) mSv (Fig. 12d).

## 6 Intercomparison with other ocean reanalysis datasets

Figure 14 shows the intercomparison of the ITF transports in the Makassar Strait among the SODA3.3.0 (without data assimilation), ensemble mean of the SODA3 (excluding the SODA3.3.0), SODA2.0.2, SODA2.2.4, ORA-S3, ORAS4, and HYCOM. The SODA3 ensemble mean (excluding SODA3.3.0), ORAS4 and HYCOM have produced annual mean volume transport of approximately (–11.29 ± 3.01) Sv, (–11.9 ± 3.08) Sv, and (–11.47 ± 4.64)

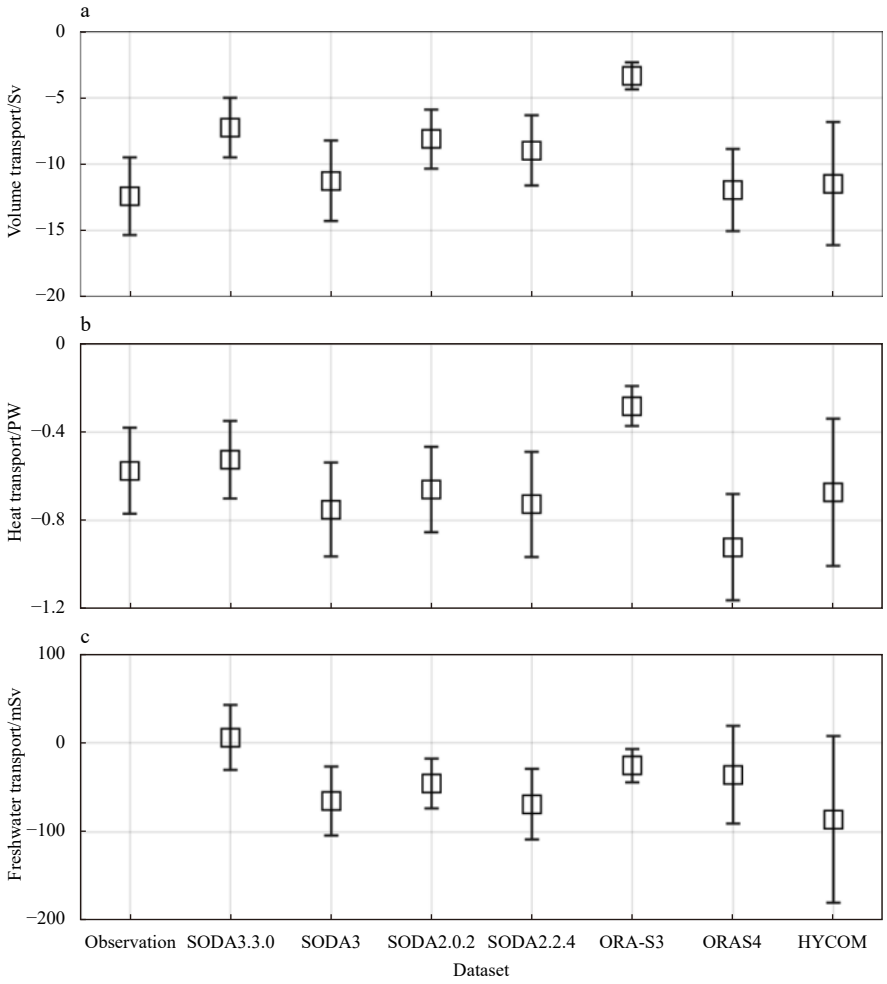


**Fig. 14.** Annual mean transport of volume (a), heat (b), and freshwater (c) in the upper 700 m of the Makassar Strait in observations and ocean reanalysis products. Error bars indicate the standard deviation of the monthly transport time series.

Sv, which are the closest to the observation. The ORA-S3 has produced the smallest annual mean volume transport ((−3.36 ± 1.02) Sv). The heat transport simulated by the SODA3.3.0 is the closest to observation, with value of (−0.53 ± 0.18) PW. The minimum and maximum simulated heat transports are (−0.28 ± 0.09) PW and (−0.92 ± 0.24) PW, given by ORA-S3 and ORAS4, respectively. There is no observed freshwater transport available, and the HYCOM gives the greatest annual mean freshwater transport ((−86.09 ± 93.66) mSv). In addition, the HYCOM also shows greatest standard deviations of 4.64 Sv, 0.33 PW, and 93.66 mSv for the volume, heat, and freshwater transports.

The analyzed ocean reanalysis products have basically reproduced the annual cycle of the volume transport, showing enhanced/weakened ITF during the southeast/northwest monsoon periods. However, only the high resolution HYCOM product has clearly simulated the semi-annual variability of the ITF volume transport in the Makassar Strait, as revealed by the double peaks of −12.46 Sv in March and −14.06 Sv in September, respectively (Fig. 15a). The annual cycle of the heat transports are generally follow that of volume transport in the ocean reanalysis products, which are not in agreement with that in observation (Fig. 15b). The simulated ITF freshwater transports in the Makassar Strait are disperse or even out of phase with each other, and cannot be validated because of no observation of salinity time series is available in the Makassar Strait (Fig. 15c). The interannual variability of the ITF transport in different ocean reanalysis products generally do not match with each other, and we do not show them here because of the analyzed ocean reanalysis products here only overlap a short period.

## 7 Discussion and conclusions

In this study, we investigate the simulated ITF in Makassar Strait in the SODA3 products by comparing with the direct measurement obtained from the INSTANT and MITF moorings. A total of nine ensemble members of the SODA3 datasets, which are forced by different surface fluxes and bulk formulas, are used for analysis. The vertical structure of subsurface velocity maximum is well reproduced by the SODA3 datasets, with ensemble mean value of (0.75 ± 0.17) m/s at 120 m depth, greater than that in observation (~0.63 m/s). The surface forcing and bulk formula influence the annual mean volume transport in the upper 728 m in the Makassar Strait. The combination of MERRA2 and Large-Yeager result in smaller volume transport, which are (−7.24 ± 1.06) Sv in SODA3.3.0 (without data assimilation) and (−9.23 ± 1.29) Sv in SODA3.3.1 (with data assimilation). The combination of MERRA2 and COARE4 (SODA3.3.2), ERA-Interim with Large-Yeager (SODA3.4.1) or COARE4 (SODA3.4.2), COREv2 and Large-Yeager (SODA3.6.1), JRA-55 (SODA3.7.2) or DFS5.2 (SODA3.11.2) or JRA-55DO (SODA3.12.2) with COARE4, roughly produce comparable annual mean volume transport, with values from (−11.05

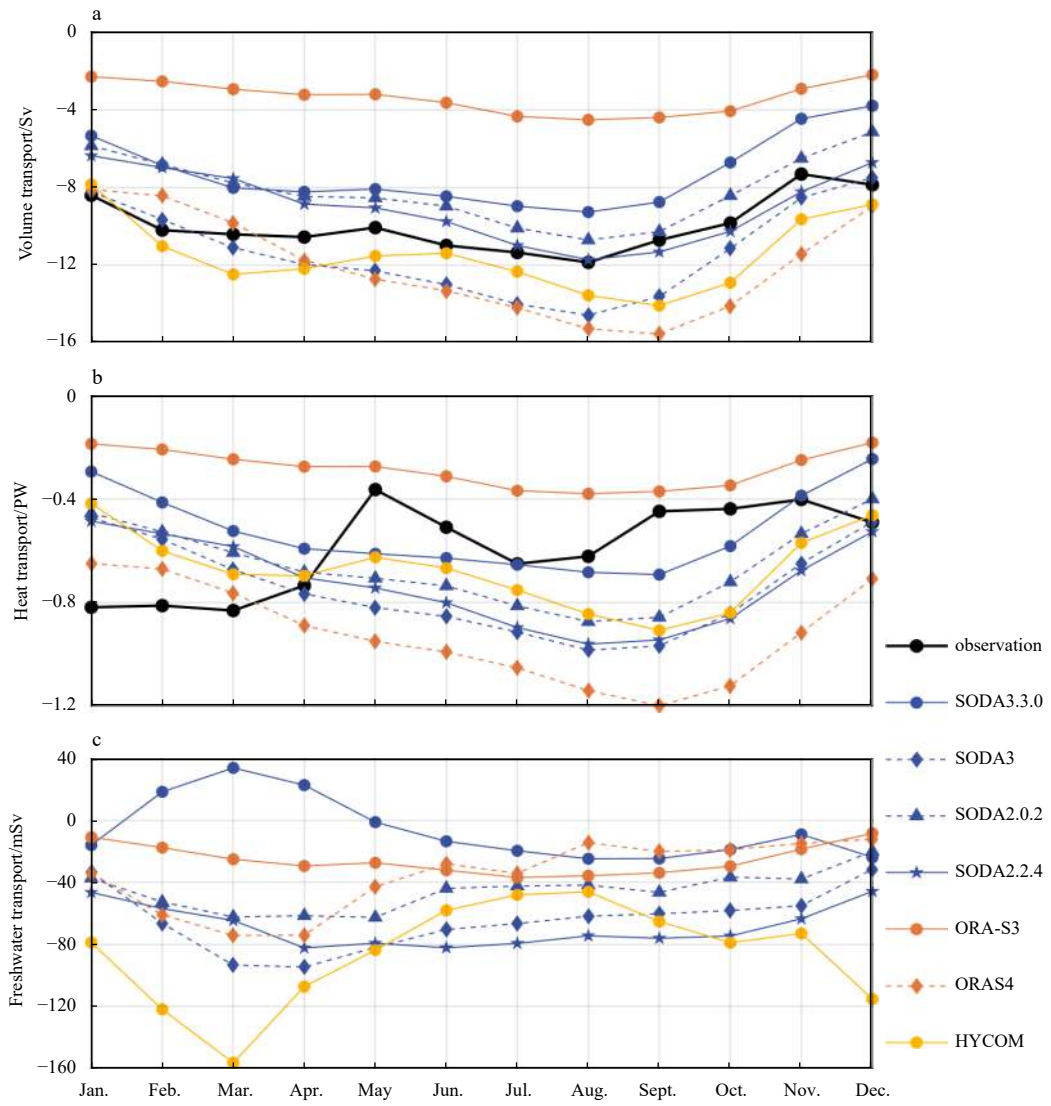


**Fig. 15.** Seasonal cycle of the depth integrated transport of volume (a), heat (b), and freshwater (c) in the upper 700 m of the Makassar Strait in observations and ocean reanalysis products.

± 1.46) Sv (SODA3.4.1) to (−11.93 ± 1.03) Sv (SODA3.6.1). The SODA3.3.0 (−0.53 ± 0.07) PW also produces the smallest heat transport. However, the relatively ranks of heat and freshwater transports are not always consistent with that of volume transport. For example, the SODA3.12.2 (−0.79 ± 0.09) PW, instead of SODA3.6.1 (−0.78 ± 0.07) PW, produces the largest heat transport; the SODA3.7.2 (−74.27 ± 21.65) mSv, instead of SODA3.6.1 (−70.53 ± 20.01) mSv, produces the largest heat transport. The SODA3.3.0 produces positive annual mean freshwater transport (6.24 ± 18.45) mSv, suggesting artificially higher salinity in the Makassar Strait without data assimilation.

The ITF vertical structure and its variations in the Makassar Strait could be decomposed into three modes: the intraseasonal and semi-annual modes that associated with Indian Ocean Kelvin waves (Mode 1), the interannual mode that associated with the ENSO modulation of Rossby waves from the Pacific (Mode 2), and the seasonal mode that associated with local monsoon wind driven (Mode 3) (Susanto et al., 2012). The monthly SODA3 datasets used in this study are not able to capture the intraseasonal mode. In terms of the semi-annual variability, they are not appropriately reproduced by all of the SODA3 ensemble members. Nevertheless, the SODA3 products have well simulated the seasonal cycle of the Makassar Strait volume transport, i.e., intensified during boreal summer and maximum in August with value of (−13.96 ± 2.10) Sv, and weakened during boreal winter and minimum in December with value of (−7.08 ± 1.40) Sv. The seasonal viability of the heat transport is in phase with that of volume transport, approximately of (−0.95 ± 0.12) and (−0.45 ± 0.09) PW in August and December, respectively. In comparison, the freshwater transport is not in phase with that of volume transport, which reaches its maximum value of (−86.79 ± 21.62) mSv in March, and minimum value of (−25.46 ± 20.71) mSv in December. This seasonal cycle in freshwater transport is basically reasonable, as evidenced by the fact that the salinity is at its lowest values in January-February-March due to heavy monsoon rainfall and advection from the South China Sea, whereas highest values in July-August-September (Fang et al., 2010; Gordon et al., 2012; Susanto et al., 2012; Wang et al., 2019; Xu et al., 2021).

Previous investigations suggest that ITF is influenced by both the ENSO and IOD anomalies (Yuan et al., 2013; Sprintall and Révelard, 2014; Liu et al., 2015). The ITF volume transport cross the IX1 section lags the Niño3.4 by around 7–9 months, which

tend to decrease/increase following the El Niño/La Niña events; and lags the DMI by around 1–3 months, which tend to decrease/increase following the negative/positive IOD events (Yuan et al., 2013; Liu et al., 2015). The water pathway from Makassar Strait to the IX1 section is not straightforward (Feng et al., 2018), and is suggested to reside in the Banda Sea for around 1 year before export to the Timor Sea (Gordon et al., 2010), and takes 2–3 years to reach the IX1 region (Song et al., 2004). The ITF in the outflow strait is slaved by the IOD anomaly rather than ENSO (Sprintall and Révelard, 2014). Susanto et al. (2012) and Gordon et al. (2019) reveal that both the ENSO and IOD could impact on the Makassar Strait throughflow, in terms of both the volume transport, and vertical velocity structure. The SODA3 simulated upper 700 m volume transport anomalies well fit with observation during periods of 2004–2017. Over the simulation period (1980–2015), the volume transport anomalies are significantly correlated with the Niño3.4 indices at time lags of –6 to 7 months, with maximum correlation coefficient of 0.50 ± 0.07 at zero-time lag. However, there are weak and insignificant correlations (smaller than 0.15 at time lag within one year) between the volume transport anomalies and the DMI indices. The heat transport in Makassar Strait displays similar seasonal and interannual variability with the volume transport, in agreement with that estimated from observation (Gruenburg and Gordon, 2018). The freshwater transport anomalies are not statistically significantly correlated with the Niño3.4/DMI indices. There is limited observation of salinity time series in the Makassar Strait to validate the freshwater transport variability at interannual timescale. Existed investigations give possible explanations of the interannual variability of salinity in the Makassar Strait. Their results suggest that the ENSO impact on the surface low salinity and subsurface high salinity waters in the Makassar Strait are not directly. Rather, the interannual signals in the surface are carried by the South China Sea throughflow (Gordon et al., 2012; Wei et al., 2016; Li et al., 2019), whereas in the subsurface is from the equatorial North Pacific with a time lag of around 2 years (Gordon et al., 2012; Nie et al., 2019). The low salinity waters carried by the South China Sea throughflow, together with the local rainfall and runoff, essentially modulate the Makassar Strait throughflow, i.e., the total volume transport and subsurface velocity maximum, at the seasonal to decadal time scales (Fang et al., 2010; Gordon et al., 2012; Hu and Sprintall, 2016, 2017; Lee et al., 2019; Li et al., 2019; Jiang et al., 2019; Wei et al., 2019; Wang et al., 2019; Xu et al., 2021). In addition to the regional surface forcing, the remote Atlantic Meridional Overturning Circulation (AMOC) also affect the ITF changes at long time scale. The mechanism is explained as: slowdown signals of the AMOC propagate through the coastal-equatorial waveguide to enter the southeastern tropical Indian Ocean and the western Pacific Ocean, which in turn result in ITF weaken in deep layers (Peng et al., 2023).

In summary, the simulated ITF in the Makassar Strait show good consistency for seasonal and interannual variability in terms of phases among the SODA3 ensemble members, and are basically in agreement with the observation. The discrepancies lie in the semi-annual variability and annual mean values. The semi-annual variability shows different upward propagation of Kelvin wave phases among the SODA3 ensemble members. The annual mean volume transport in SODA3.3.0 and SODA3.3.1 are obviously smaller than others, which may attribute to different surface forcings and bulk formulas. The annual mean freshwater transport in SODA3.3.0 (without data assimilation) is positive, which is opposite to the rest ensemble members (with data assimilation). There is heavy rainfall in the Indo-Pacific warm pool where the ITF pass through. Therefore, the salinity simulation tends to more sensitive and important in the ITF regions. Consequently, the ITF transport, particularly for the freshwater transport shows dramatically differences between the non-data assimilated SODA3.3.0 and those with data assimilation. The unreasonable freshwater transport in SODA3.3.0 suggest that the data assimilation is necessary and effective in the SODA3 coordinate. The relationships of the Makassar Strait transports with ENSO and IOD are analyzed, showing significant correlation with ENSO but no significant correlation with IOD. For the interannual heat and freshwater transports, they are contributed by both the velocity and temperature or salinity anomalies. The velocity and temperature anomalies contribute 87% and 8% of the interannual variation of the heat transport. For the freshwater transport, the contributions of velocity and salinity anomalies are 41% and 56%, respectively. In addition, we give a short intercomparison of SODA3 with other ocean reanalysis products. The results show improved simulation of the ITF transports by the high resolution HYCOM, particularly in terms of the semi-annual variability.

***Acknowledgements***

CCMP Version-3.0 vector wind analyses are produced by Remote Sensing Systems, available at www.remss.com. The SODA3 datasets are provided by the University of Maryland, available at https://www2.atmos.umd.edu/~ocean/. We appreciate Liwei Wang and Dawei Li for conducting the collection and formal process and analysis of the data, and cherish the memory of them.

**References**

Atlas R, Hoffman R N, Ardizzone J, et al. 2011. A cross-calibrated, multiplatform ocean surface wind velocity product for meteorological and oceanographic applications. Bulletin of the American Meteorological Society, 92(2): 157–174, doi: 10.1175/2010BAMS2946.1

Balmaseda M A, Mogensen K, Weaver A T. 2013. Evaluation of the ECMWF ocean reanalysis system ORAS4. Quarterly Journal of the Royal Meteorological Society, 139(674): 1132–1161, doi: 10.1002/qj.2063

Balmaseda M A, Vidard A, Anderson D L T. 2008. The ECMWF ocean analysis system: ORA-S3. Monthly Weather Review, 136(8): 3018–3034, doi: 10.1175/2008MWR2433.1

Bleck R, Boudra D B. 1981. Initial testing of a numerical ocean circulation model using a hybrid (quasi-isopycnic) vertical coordinate. Journal of Physical Oceanography, 11(6): 755–770, doi: 10.1175/1520-0485(1981)011<0755:ITOANO>2.0.CO;2

Boyer T P, Antonov J I, Baranova O K, et al. 2013. World ocean database 2013. Silver Spring: National Oceanographic Data Center Ocean Climate Laboratory

Broecker W S. 1991. The great ocean conveyor. Oceanography, 4(2): 79–89, doi: 10.5670/oceanog.1991.07

Carton J A, Chepurin G A, Chen Ligang. 2018. SODA3: a new ocean climate reanalysis. Journal of Climate, 31(17): 6967–6983, doi: 10.1175/JCLI-D-18-0149.1

Carton J A, Giese B S. 2008. A reanalysis of ocean climate using Simple Ocean Data Assimilation (SODA). Monthly Weather Review, 136(8): 2999–3017, doi: 10.1175/2007MWR1978.1

Casey K S, Brandon T B, Cornillon P, et al. 2010. The past, present, and future of the AVHRR Pathfinder SST Program. In: Barale V, Gower J F R, Alberotanza L, eds. Oceanography from Space: Revisited. Dordrecht: Springer, 273–287, doi: 10.1007/978-90-481-8681-5_16

Dee D P, Uppala S M, Simmons A J, et al. 2011. The ERA-Interim reanalysis: configuration and performance of the data assimilation system. Quarterly Journal of the Royal Meteorological Society, 137(656): 553–597, doi: 10.1002/qj.828

Delworth T L, Rosati A, Anderson W, et al. 2012. Simulated climate and climate change in the GFDL CM2.5 high-resolution

coupled climate model. Journal of Climate, 25(8): 2755–2781, doi: 10.1175/JCLI-D-11-00316.1

Du Yan, Qu Tangdong. 2010. Three inflow pathways of the Indonesian throughflow as seen from the simple ocean data assimilation. Dynamics of Atmospheres and Oceans, 50(2): 233–256, doi: 10.1016/j.dynatmoce.2010.04.001

Dussin R, Barnier B, Brodeau L, et al. 2016. The making of the DRAKKAR FORCING SET DFS5. Grenoble, France: Laboratoire de Glaciologie et Géophysique de l'Environnement

Fairall C W, Bradley E F, Hare J E, et al. 2003. Bulk parameterization of air-sea fluxes: updates and verification for the COARE algorithm. Journal of Climate, 16(4): 571–591, doi: 10.1175/1520-0442(2003)016<0571:BPOASF>2.0.CO;2

Fang Guohong, Susanto R D, Wirasantosa S, et al. 2010. Volume, heat, and freshwater transports from the South China Sea to Indonesian seas in the boreal winter of 2007–2008. Journal of Geophysical Research: Oceans, 115(C12): C12020, doi: 10.1029/2010JC006225

Feng Ming, Zhang Ningning, Liu Qinyan, et al. 2018. The Indonesian throughflow, its variability and centennial change. Geoscience Letters, 5(1): 3, doi: 10.1186/s40562-018-0102-2

Gelaro R, McCarty W, Suárez M J, et al. 2017. The modern-era retrospective analysis for research and applications, version 2 (MERRA-2). Journal of Climate, 30(14): 5419–5454, doi: 10.1175/JCLI-D-16-0758.1

Godfrey J S. 1989. A Sverdrup model of the depth-integrated flow for the world ocean allowing for island circulations. Geophysical & Astrophysical Fluid Dynamics, 45(1–2): 89–112, doi: 10.1080/03091928908208894

Gordon A L. 1986. Interocean exchange of thermocline water. Journal of Geophysical Research: Oceans, 91(C4): 5037–5046, doi: 10.1029/JC091iC04p05037

Gordon A L. 2005. Oceanography of the Indonesian seas and their throughflow. Oceanography, 18(4): 14–27, doi: 10.5670/oceanog.2005.01

Gordon A L, Fine R A. 1996. Pathways of water between the Pacific and Indian oceans in the Indonesian seas. Nature, 379(6561): 146–149, doi: 10.1038/379146a0

Gordon A L, Huber B A, Metzger E J, et al. 2012. South China Sea throughflow impact on the Indonesian throughflow. Geophysical Research Letters, 39(11): L11602, doi: 10.1029/2012GL052021

Gordon A L, Napitu A, Huber B A, et al. 2019. Makassar Strait throughflow seasonal and interannual variability: an overview. Journal of Geophysical Research: Oceans, 124(6): 3724–3736, doi: 10.1029/2018JC014502

Gordon A L, Sprintall J, Van Aken H M, et al. 2010. The Indonesian throughflow during 2004–2006 as observed by the INSTANT program. Dynamics of Atmospheres and Oceans, 50(2): 115–128, doi: 10.1016/j.dynatmoce.2009.12.002

Gordon A L, Susanto R D, Ffield A. 1999. Throughflow within Makassar Strait. Geophysical Research Letters, 26(21): 3325–3328, doi: 10.1029/1999GL002340

Griffies S M, Biastoch A, Böning C, et al. 2009. Coordinated ocean-ice reference experiments (COREs). Ocean Modelling, 26(1–2): 1–46, doi: 10.1016/j.ocemod.2008.08.007

Gruenburg L K, Gordon A L. 2018. Variability in Makassar Strait heat flux and its effect on the eastern tropical Indian Ocean. Oceanography, 31(2): 80–87, doi: 10.5670/oceanog.2018.220

Harada Y, Kamahori H, Kobayashi C, et al. 2016. The JRA-55 Reanalysis: representation of atmospheric circulation and climate variability. Journal of the Meteorological Society of Japan, 94(3): 269–302, doi: 10.2151/jmsj.2016-015

Hirst A C, Godfrey J S. 1993. The role of Indonesian throughflow in a global ocean GCM. Journal of Physical Oceanography, 23(6): 1057–1086, doi: 10.1175/1520-0485(1993)023<1057:TROITI>2.0.CO;2

Hu Shijian, Sprintall J. 2016. Interannual variability of the Indonesian Throughflow: the salinity effect. Journal of Geophysical Research: Oceans, 121(4): 2596–2615, doi: 10.1002/2015jc011495

Hu Shijian, Sprintall J. 2017. Observed strengthening of interbasin exchange via the Indonesian seas due to rainfall intensification. Geophysical Research Letters, 44(3): 1448–1456, doi: 10.1002/2016gl072494

Humphries U W, Webb D J. 2008. On the Indonesian Throughflow in the OCCAM 1/4 degree ocean model. Ocean Science, 4(3): 183–198, doi: 10.5194/os-4-183-2008

Ilahude A G, Gordon A L. 1996. Thermocline stratification within the Indonesian Seas. Journal of Geophysical Research: Oceans, 101(C5): 12401–12409, doi: 10.1029/95JC03798

Jiang Guoqing, Wei Jun, Malanotte-Rizzoli P, et al. 2019. Seasonal and interannual variability of the subsurface velocity profile of the Indonesian throughflow at Makassar Strait. Journal of Geophysical Research: Oceans, 124(12): 9644–9657, doi: 10.1029/2018jc014884

Kobayashi S, Ota Y, Harada Y, et al. 2015. The JRA-55 Reanalysis: general specifications and basic characteristics. Journal of the Meteorological Society of Japan, 93(1): 5–48, doi: 10.2151/jmsj.2015-001

Large W G, Yeager S G. 2004. Diurnal to decadal global forcing for ocean and sea-ice models: the data sets and flux climatologies. Boulder: University Corporation for Atmospheric Research. doi: 10.5065/D6KK98Q6

Large W G, Yeager S G. 2009. The global climatology of an interannually varying air–sea flux data set. Climate Dynamics, 33(2): 341–364, doi: 10.1007/s00382-008-0441-3

Lee T, Awaji T, Balmaseda M, et al. 2010. Consistency and fidelity of Indonesian-throughflow total volume transport estimated by 14 ocean data assimilation products. Dynamics of Atmospheres and Oceans, 50(2): 201–223, doi: 10.1016/j.dynatmoce.2009.12.004

Lee T, Fournier S, Gordon A L, et al. 2019. Maritime Continent water cycle regulates low-latitude chokepoint of global ocean circulation. Nature Communications, 10(1): 2103, doi: 10.1038/s41467-019-10109-z

Li Mingting, Gordon A L, Gruenburg L K, et al. 2020. Interannual to decadal response of the Indonesian Throughflow vertical profile to Indo-Pacific forcing. Geophysical Research Letters, 47(11): e2020GL087679, doi: 10.1029/2020GL087679

Li Mingting, Wei Jun, Wang Dongxiao, et al. 2019. Exploring the importance of the Mindoro-Sibutu pathway to the upper-layer circulation of the South China Sea and the Indonesian throughflow. Journal of Geophysical Research: Oceans, 124(7): 5054–5066, doi: 10.1029/2018jc014910

Liang Linlin, Xue Huijie, Shu Yeqiang. 2019. The Indonesian throughflow and the circulation in the Banda Sea: a modeling study. Journal of Geophysical Research: Oceans, 124(5): 3089–3106, doi: 10.1029/2018JC014926

Liu Yun, Feng Ming, Church J, et al. 2005. Effect of salinity on estimating geostrophic transport of the Indonesian throughflow along the IX1 XBT section. Journal of Oceanography, 61(4): 795–801, doi: 10.1007/s10872-005-0086-3

Liu Qinyan, Feng Ming, Wang Dongxiao, et al. 2015. Interannual variability of the Indonesian Throughflow transport: a revisit based on 30 year expendable bathythermograph data. Journal of Geophysical Research: Oceans, 120(12): 8270–8282, doi: 10.1002/2015JC011351

Mears C A, Scott J, Wentz F J, et al. 2019. A near-real-time version of the cross-calibrated multiplatform (CCMP) ocean surface wind velocity data set. Journal of Geophysical Research: Oceans, 124(10): 6997–7010, doi: 10.1029/2019JC015367

Metzger E J, Hurlburt H E, Xu Xiaobiao, et al. 2010. Simulated and observed circulation in the Indonesian Seas: 1/12° global HYCOM and the INSTANT observations. Dynamics of Atmospheres and Oceans, 50(2): 275–300, doi: 10.1016/j.dynatmoce.2010.04.002

Meyers G, Bailey R J, Worby A P. 1995. Geostrophic transport of Indonesian Throughflow. Deep-Sea Research Part I: Oceanographic Research Papers, 42(7): 1163–1174, doi: 10.1016/0967-0637(95)00037-7

Napitu A M, Pujiana K, Gordon A L. 2019. The Madden-Julian Oscillation's impact on the Makassar Strait surface layer transport. Journal of Geophysical Research: Oceans, 124(6): 3538–3550,

doi: 10.1029/2018JC014729
Nie Xunwei, Gao Shan, Wang Fan, et al. 2019. Origins and pathways of the Pacific Equatorial Undercurrent identified by a simulated adjoint tracer. Journal of Geophysical Research: Oceans, 124(4): 2331–2347, doi: 10.1029/2018JC014212
Nur'utami M N, Hidayat R. 2016. Influences of IOD and ENSO to Indonesian rainfall variability: role of atmosphere-ocean interaction in the Indo-Pacific Sector. Procedia Environmental Sciences, 33: 196–203, doi: 10.1016/j.proenv.2016.03.070
Peng Qihua, Xie Shangping, Huang Ruixin, et al. 2023. Indonesian throughflow slowdown under global warming: remote AMOC effect versus regional surface forcing. Journal of Climate, 36(5): 1301–1318, doi: 10.1175/JCLI-D-22-0331.1
Potemra J. 2005. Indonesian Throughflow transport variability estimated from satellite altimetry. Oceanography, 18(4): 98–107, doi: 10.5670/oceanog.2005.10
Pujiana K, Gordon A L, Sprintall J. 2013. Intraseasonal Kelvin wave in Makassar Strait. Journal of Geophysical Research: Oceans, 118(4): 2023–2034, doi: 10.1002/jgrc.20069
Pujiana K, McPhaden M J. 2020. Intraseasonal Kelvin waves in the equatorial Indian ocean and their propagation into the Indonesian seas. Journal of Geophysical Research: Oceans, 125(5): e2019JC015839, doi: 10.1029/2019JC015839
Pujiana K, McPhaden M J, Gordon A L, et al. 2019. Unprecedented response of Indonesian throughflow to anomalous Indo-Pacific climatic forcing in 2016. Journal of Geophysical Research: Oceans, 124(6): 3737–3754, doi: 10.1029/2018JC014574
Saji N H, Goswami B N, Vinayachandran P N, et al. 1999. A dipole mode in the tropical Indian Ocean. Nature, 401(6751): 360–363, doi: 10.1038/43854
Schiller A, Godfrey J S, McIntosh P C, et al. 1998. Seasonal near-surface dynamics and thermodynamics of the Indian Ocean and Indonesian Throughflow in a global ocean general circulation model. Journal of Physical Oceanography, 28(11): 2288–2312, doi: 10.1175/1520-0485(1998)028<2288:SNSDAT>2.0.CO;2
Song Qian, Gordon A L, Visbeck M. 2004. Spreading of the Indonesian throughflow in the Indian Ocean. Journal of Physical Oceanography, 34(4): 772–792, doi: 10.1175/1520-0485(2004)034<0772:SOTITI>2.0.CO;2
Sprintall J, Gordon A L, Wijffels S E, et al. 2019. Detecting change in the Indonesian seas. Frontiers in Marine Science, 6: 257, doi: 10.3389/fmars.2019.00257
Sprintall J, Révelard A. 2014. The Indonesian throughflow response to Indo-Pacific climate variability. Journal of Geophysical Research: Oceans, 119(2): 1161–1175, doi: 10.1002/2013JC009533
Sprintall J, Wijffels S, Gordon A L, et al. 2004. INSTANT: a new international array to measure the Indonesian Throughflow. Eos, Transactions American Geophysical Union, 85(39): 369–376, doi: 10.1029/2004EO390002
Sprintall J, Wijffels S E, Molcard R, et al. 2009. Direct estimates of the Indonesian Throughflow entering the Indian Ocean: 2004–2006. Journal of Geophysical Research: Oceans, 114(C7): C07001, doi: 10.1029/2008JC005257
Susanto R D, Ffield A, Gordon A L, et al. 2012. Variability of Indonesian throughflow within Makassar Strait, 2004–2009. Journal of Geophysical Research: Oceans, 117(C9): C09013, doi: 10.1029/2012JC008096
Susanto R D, Gordon A L. 2005. Velocity and transport of the Makassar Strait throughflow. Journal of Geophysical Research: Oceans, 110(C1): C01005, doi: 10.1029/2004JC002425
Susanto R D, Song Y T. 2015. Indonesian throughflow proxy from satellite altimeters and gravimeters. Journal of Geophysical Research: Oceans, 120(4): 2844–2855, doi: 10.1002/2014jc010382
Susanto R D, Wei Zexun, Adi R T, et al. 2013. Observations of the Karimata Strait throughflow from December 2007 to November 2008. Acta Oceanologica Sinica, 32(5): 1–6, doi: 10.1007/s13131-013-0307-3
Talley L D. 2013. Closure of the global overturning circulation through the Indian, Pacific, and Southern Oceans: schematics and transports. Oceanography, 26(1): 80–97, doi: 10.5670/oceanog.2013.07
Tillinger D, Gordon A L. 2009. Fifty years of the Indonesian throughflow. Journal of Climate, 22(23): 6342–6355, doi: 10.1175/2009JCLI2981.1
Tillinger D, Gordon A L. 2010. Transport weighted temperature and internal energy transport of the Indonesian throughflow. Dynamics of Atmospheres and Oceans, 50(2): 224–232, doi: 10.1016/j.dynatmoce.2010.01.002
Tsujino H, Urakawa S, Nakano H, et al. 2018. JRA-55 based surface dataset for driving ocean–sea-ice models (JRA55-do). Ocean Modelling, 130: 79–139, doi: 10.1016/j.ocemod.2018.07.002
van Sebille E, Sprintall J, Schwarzkopf F U, et al. 2014. Pacific-to-Indian Ocean connectivity: Tasman leakage, Indonesian Throughflow, and the role of ENSO. Journal of Geophysical Research: Oceans, 119(2): 1365–1382, doi: 10.1002/2013JC009525
Wang Yan, Xu Tengfei, Li Shujiang, et al. 2019. Seasonal variation of water transport through the Karimata Strait. Acta Oceanologica Sinica, 38(4): 47–57, doi: 10.1007/s13131-018-1224-2
Wei Jun, Li Mingting, Malanotte-Rizzoli P, et al. 2016. Opposite variability of Indonesian Throughflow and South China Sea throughflow in the Sulawesi Sea. Journal of Physical Oceanography, 46(10): 3165–3180, doi: 10.1175/jpo-d-16-0132.1
Wei Zexun, Li Shujiang, Susanto R D, et al. 2019. An overview of 10-year observation of the South China Sea branch of the Pacific to Indian Ocean throughflow at the Karimata Strait. Acta Oceanologica Sinica, 38(4): 1–11, doi: 10.1007/s13131-019-1410-x
Wijffels S E, Meyers G, Godfrey J S. 2008. A 20-Yr average of the Indonesian throughflow: regional currents and the interbasin exchange. Journal of Physical Oceanography, 38(9): 1965–1978, doi: 10.1175/2008jpo3987.1
Woodruff S D, Worley S J, Lubker S J, et al. 2011. ICOADS Release 2.5: extensions and enhancements to the surface marine meteorological archive. International Journal of Climatology, 31(7): 951–967, doi: 10.1002/joc.2103
Wyrtki K. 1961. Physical Oceanography of the Southeast Asian Waters. La Jolla: Scripps Institution of Oceanography
Wyrtki K. 1987. Indonesian through flow and the associated pressure gradient. Journal of Geophysical Research: Oceans, 92(C12): 12941–12946, doi: 10.1029/JC092iC12p12941
Xie Tengxiang, Newton R, Schlosser P, et al. 2019. Long-term mean mass, heat and nutrient flux through the Indonesian seas, based on the tritium inventory in the Pacific and Indian oceans. Journal of Geophysical Research: Oceans, 124(6): 3859–3875, doi: 10.1029/2018jc014863
Xu Tengfei, Wei Zexun, Susanto R D, et al. 2021. Observed water exchange between the South China Sea and Java Sea through Karimata Strait. Journal of Geophysical Research: Oceans, 126(2): e2020JC016608, doi: 10.1029/2020JC016608
Yuan Dongliang, Zhou Hui, Zhao Xia. 2013. Interannual climate variability over the tropical Pacific Ocean induced by the Indian Ocean dipole through the Indonesian Throughflow. Journal of Climate, 26(9): 2845–2861, doi: 10.1175/jcli-d-12-00117.1
Zhang Tiecheng, Wang Weiqiang, Xie Qiang, et al. 2019. Heat contribution of the Indonesian throughflow to the Indian Ocean. Acta Oceanologica Sinica, 38(4): 72–79, doi: 10.1007/s13131-019-1414-6
Zhao Yunxia, Wei Zexun, Wang Yonggang, et al. 2015. Correlation analysis of the North Equatorial Current bifurcation and the Indonesian Throughflow. Acta Oceanologica Sinica, 34(9): 1–11, doi: 10.1007/s13131-015-0736-2